

# **Spatial variability in surface water-groundwater fluxes using hydraulic methods**

Saskia L. Noorduijn

M. Eng. Sc., University of Western Australia

B. Sc. (Hons), University of Aberdeen

This thesis is submitted as requirement in  
full for the degree of Doctor of Philosophy

School of the Environment  
Faculty of Science and Engineering  
Flinders University of South Australia

Feb 2014



# Contents

<b>List of Figures</b>	<b>v</b>
<b>List of Tables</b>	<b>xi</b>
<b>Declaration</b>	<b>xiii</b>
<b>Co-Authorship</b>	<b>xv</b>
<b>Acknowledgements</b>	<b>xvii</b>
<b>Summary</b>	<b>xix</b>
<b>1 Introduction</b>	<b>1</b>
1.1 Background . . . . .	1
1.2 Research aims . . . . .	3
<b>2 The representative stream length for estimating surface water - groundwater exchange using Darcy's Law</b>	<b>5</b>
2.1 Abstract . . . . .	6
2.2 Introduction . . . . .	6
2.3 Numerical simulations . . . . .	8
2.3.1 Model conceptualization and set up . . . . .	9
2.3.1.1 Synthetic aquifers . . . . .	9
2.3.1.2 Model Design . . . . .	10
2.3.1.3 Steady state groundwater discharge . . . . .	11
2.3.1.4 Stream stage response to estimate $K_{eff}$ and $Q_{eff}$ . . . . .	13
2.3.2 Model Results . . . . .	15
2.3.2.1 Variability in $Q_{eff}$ versus piezometer distance . . . . .	15
2.3.2.2 Comparison of measurement scales . . . . .	18

2.4	Example of field application . . . . .	19
2.4.1	Field setting . . . . .	19
2.4.2	Calculation of $K_{eff}$ . . . . .	20
2.4.3	Variability in estimated $K_{eff}$ and $Q_{eff}$ . . . . .	22
2.5	Discussion . . . . .	23
2.6	Conclusions . . . . .	25

**3 Estimating seepage flux from ephemeral stream channels using surface and ground-water level data 27**

3.1	Abstract . . . . .	28
3.2	Introduction . . . . .	28
3.3	Background . . . . .	31
3.3.1	Theory . . . . .	31
3.3.2	Field Site . . . . .	34
3.4	Methodology . . . . .	35
3.4.1	Field Methods . . . . .	35
3.4.2	Modeling . . . . .	37
3.4.2.1	Model Calibration . . . . .	40
3.4.2.2	Sensitivity Analysis . . . . .	41
3.5	Results . . . . .	42
3.5.1	Experimental Results . . . . .	42
3.5.2	Model Results . . . . .	43
3.5.3	Monte Carlo Sensitivity Analysis Results . . . . .	46
3.6	Discussion . . . . .	50
3.7	Conclusions . . . . .	52

**4 Using sealed wells to measure water levels beneath streams and floodplains 55**

4.1	Abstract . . . . .	56
4.2	Introduction . . . . .	56
4.3	Theory . . . . .	58
4.4	Methodolgy . . . . .	61

4.4.1	Laboratory setup . . . . .	61
4.4.2	Experimental design . . . . .	61
4.5	Results . . . . .	62
4.6	Discussion . . . . .	64
4.7	Conclusion . . . . .	66
<b>5</b>	<b>Conclusions</b>	<b>67</b>
5.1	Overview . . . . .	67
5.2	Future work . . . . .	68
	<b>Bibliography</b>	<b>71</b>
	<b>Appendices</b>	
<b>A</b>	<b>Analytical model validation</b>	<b>89</b>
<b>B</b>	<b>Further Discussion of Sensitivity Analysis</b>	<b>91</b>
B.1	Distribution of sensitivity analysis results in Figure 3.8 . . . . .	91
B.2	Assymetry in $\phi$ values for $S_y$ . . . . .	91
B.3	Calibrated model $\phi$ values compared to the sensitivity analysis $\phi$ results .	92
B.4	Discussion on the impact of Manning's $n$ . . . . .	93
<b>C</b>	<b>Field data</b>	<b>95</b>



# List of Figures

2.1	Examples of the synthetically generated K fields with different variances ( $\sigma^2$ ) and correlation length ( $\tau$ ). (a) $\sigma^2 = 1.0$ and $\tau = 10$ m, (b) $\sigma^2 = 4.5$ and $\tau = 10$ m, (c) $\sigma^2 = 1.0$ and $\tau = 100$ m, and (d) $\sigma^2 = 4.5$ and $\tau = 100$ m.	9
2.2	(a) Schematic of the model set up and location of the observation wells (unfilled circles). Constant head boundary on the right ( $h_2=9.0$ m) and a time variant head boundary on the left which represents the stream ( $h_1(t_0)=8.5$ m, $h_1(t_1)=7.0$ m). (b) shows how the discharge estimates derived from the analytical solution are related to the modeled stream discharge from the MODFLOW model. For clarity, only a selected number of length are shown. Refer to section 2.2.1.3, Eq. 2.1 and Table 2.1 for parameter descriptions.	11
2.3	Examples of the distribution of the correlation coefficient between $Q_{eff}^{x,y}$ and $Q_l^y$ for different equivalent stream discharge length ( $l_{equ}$ ) (m).	12
2.4	The spread in groundwater discharge estimates related to the observation well distance for 30 aquifer realizations with a variance = 1.0 and correlation length = 50 m.	15
2.5	Variability in the Darcy's law groundwater discharge ( $CV(Q_{eff}^{x,y})$ ) as a function of the observation well distance for two different $\ln(K)$ variances.	16
2.6	Darcy's law groundwater discharge variability ( $CV(Q_{eff}^{x,y})$ ) as a function of the ratio of the observation well distance to the correlation length ( $x/\tau$ ), shown for two different $\ln(K)$ variances.	17
2.7	Changes in the estimated representative stream discharge length as a function of the observation well distance based on Darcy's law groundwater discharge ( $Q_{eff}^{x,y}$ ) and numerical groundwater discharge ( $Q^y$ ), (a) for an aquifer with $\sigma^2 = 1.0$ and (b) $\sigma^2 = 4.5$ . The error bars are the standards deviation in the equivalent stream discharge length for the 30 realizations.	18

2.8 Map of the Fairview Drain experimental site showing the Fairview Drain, the location and ID for all observation wells (circles), location of the flow regulator, and the steady state groundwater contours (blue) in m AHD. . . . . 20

2.9 Calibration of the observation well data using MODFLOW (assuming 10% stream penetration) and PEST for the stage change experiments on (a) 15 Oct 2011 and (b) on 10 Oct 2012 respectively. The stream stage (solid gray line), the observed (circles) and the calibrated MODFLOW modeling fit (dashed line) are presented. Examples of both the best and worst calibration fits for the observation data are shown. For clarity, only two locations and part of the measured data points are shown. . . . . 21

2.10 Influence of stream-aquifer penetration (5% and 10%) on the calibrated effective hydraulic conductivity ( $K_{eff}$ ) and steady state groundwater discharge ( $Q_{eff}$ ) as a function of the observation well distance.  $K_{eff}$  represent the geometric mean of the  $K_{eff}$  for each observation well determined from the MODFLOW model for both stage change experiments at the Fairview Drain experimental site. . . . . 22

3.1 Conceptual diagram of the diffusion wave - MODFLOW model (based on Niswonger et al. (2008)) showing the surface and subsurface discretization for flow calculation, where  $A$  is channel area ( $L^2$ ) and  $Q$  is flow ( $L^3T^{-1}$ ). . . . . 31

3.2 Map of the Western Reflows Floodway (WRF) study reach in the South East region of South Australia. Dashed lines define segment boundaries for the model (surface water node, see Figure 3.1) and identify the location of surface water level monitoring. Topography is shown as metres above sea level . . . . . 34

3.3	Inflow flood hydrograph determined by manual gauging at the upstream boundary of the WRF reach. The area-velocity technique was applied to determine flow. Error bars are calculated from a 5% measurement error with an additional error calculated from the change in flow during the period of each flow measurement. The total estimated error ranged from 15% at the beginning of the event to 5% for the steady state. . . . .	42
3.4	Timing and shape of the flood-wave at each segment boundary (grey diamond and labeled $S_2, S_4$ , etc) determined from pressure transducer data and site survey at each boundary. The circles and dashed line (unfilled) show the cumulative travel time of the flood front for both the initial flow (filled circles) and flow at full width inundation (open circles). . . . .	43
3.5	The root mean squared error (RMSE) associated with different data types for three different calibration scenarios (see Table 3.3). . . . .	44
3.6	Estimated seepage flux (solid circles) along the channel for each model calibration scenario. . . . .	45
3.7	Observed (OBS) and modeled (MOD) surface water levels and groundwater heads at Sites 1 and 2 (see Figure 3.2 for locations). . . . .	45
3.8	Six examples showing the impacts of changes in parameter value, expressed as given in standard deviations relative to the calibration model value, to the flood front flow ( $ff$ flow $\phi$ ), surface water stage ( $sws$ $\phi$ ), and groundwater head ( $gwh$ $\phi$ ). Modeled parameter errors and values are provided in Tables 3.1 and 3.2. For example, $LnK_s^3$ equals $-8.52$ ( $m\ s^{-1}$ ) $\pm 1$ ; therefore, when the number of $\sigma$ equals $-2, -0.5,$ and $1$ , $LnK_s^3$ equals $-10.52, -9.02$ and $-7.52$ respectively ((m), (n), and (o)). The color represents the total seepage flux ( $m^3$ ) along the channel. Stars represent the calibrated model $\phi$ and total seepage flux. . . . .	47
3.9	Flood front flow $\phi$ versus the groundwater head $\phi$ . The color represents the total seepage flux ( $m^3$ ) along the channel. Star represent the calibrated model $\phi$ . . . . .	48

3.10	Uncertainty in total seepage flux ( $m^3$ ) from the study reach associated with changes in six parameter value (given in standard deviations, $\sigma$ ) determined from the modified Monte Carlo analysis. The color represents the average $\bar{\phi}$ of the three individual for each dataset shown in Figure 3.8. The star represents the total seepage flux and $\bar{\phi}$ of the calibrated model. . . . .	49
4.1	Wells with very tall standpipes are often constructed to avoid inundation by floodwaters. This example is from the Daly River, Australia (courtesy of Steven Tickell). . . . .	57
4.2	Schematic representation of (a) a sealed well and the measurements involved in calculating the hydraulic head using a non-vented pressure transducer and (b) the experimental setup with the experiments water levels are indicated. All groundwater levels ( $h^O$ and $h^S$ for the open and sealed well respectively) are relative to the measurement point (i.e., location of the pressure transducer sensor) and all depth measurements refer to the sealed well ( $d_0$ and $d_1$ ) and are relative to the top of casing. . . . .	59
4.3	Observed response to the three level changes in the pressure transducers and capacitance probes within the open and sealed wells. (a) shows the total pressure from the non-vented pressure transducer located in the screened section of the open ( $P_T^O$ ) and sealed ( $P_T^S$ ) wells, expressed as length (m H <sub>2</sub> O). (b) shows the actual water level response monitored by the capacitance water level loggers in the open ( $h^O$ ) and sealed ( $h^S$ ) wells. The water level response in a theoretical airtight, sealed well for this experiment (calculated using Eq 3.7) is also shown ( $h^{Sim}$ ). The barometric pressure is also shown for the open (i.e., ambient barometric pressure) ( $A^O$ ) and sealed ( $A^S$ ) well, expressed as length (m H <sub>2</sub> O). . . . .	63

A.1	Influence of aquifer thickness ((a) 10 m and (b) 100 m) and stream penetration (40-100%) on determining hydraulic conductivities using the Hall and Moench (1972) analytical solution. Input data was derived from homogeneous 2-dimensional (cross sectional) aquifers simulated in MODFLOW, distance between stream and observation well was identical to the heterogeneous model. . . . .	89
B.1	The relation between flood front flow $\phi$ , surface water stage $\phi$ , and groundwater head $\phi$ (colour bar for reference). Star represents the calibrated model $\phi$ . . . . .	92



# List of Tables

2.1	Description of model parameters. . . . .	8
2.2	Statistics for the estimated $K_{eff}$ from the Fairview Drain experimental site (excluding transect 11 data). . . . .	23
3.1	Description of model parameters. Where appropriate the estimated measurement error for each parameter has been identified based on the authors judgement. . . . .	36
3.2	Parameters values for the 15 segments within the WRF study reach that were fixed during the calibration process. These values were allowed to vary during the sensitivity analysis. Refer to Table 3.1 for parameter definitions and estimated measurement error. . . . .	38
3.3	Outline of the calibration scenarios tested, where streambed hydraulic conductivity is $K_s$ , surface water level is $h_s$ , and groundwater head is $h_g$ . Manning's $n$ was allowed to vary for 10 surface water stages ( $sws$ ) for Scenario 3. . . . .	43
3.4	Mean and variance of the total seepage ( $m^3$ ) along the channel for all Monte Carlo simulation results, and where $\phi \leq 0.3$ . . . . .	49



# Declaration

I certify that this thesis does not incorporate without knowledge any material previously submitted for a degree or diploma in any other university; and that to the best of my knowledge and belief it does not contain any material previously published or written by another person except where due reference is made in the text.

A handwritten signature in black ink, reading "S.L. Noorduijn". The signature is written in a cursive style with a long horizontal stroke at the bottom. To the right of the signature is a small, light gray rectangular stamp.

Saskia L. Noorduijn



# Co-Authorship

Saskia L. Noorduij is the primary author on all manuscripts in this thesis. On all submitted papers, the co-authors provided intellectual supervision and editorial content.



# Acknowledgments

I wish to acknowledge the funding from the Australian Research Council and the National Water Commission via the National Centre for Groundwater Research and Training. Without this support, the research presented here would not have been possible. I would also like to acknowledge the Goyder Institute for Water Research of South Australia for contributing funding to site infrastructure and providing me with a scholarship top-up.

I am most grateful for the support and guidance of my supervisors Prof. Peter Cook and Dr Glenn Harrington. I have learnt a great deal over the past 3.5 years, most of it a result of their scientific guidance. Thanks to Glenn for his insight into the hydrogeology of the south east of South Australia, and for all the assistance in the field (good times!). I am indebted to Peter for his clear thinking and logical approach to research, which helped guide me through this project. I also wish to thank all the admin staff (particularly Anna Bonnes) in the NCGRT and the School of the Environment for their assistance over the years.

On a more personal note, I want to thank all the members of Program 3 for their continued enthusiasm, field assistance and friendship. My time at Flinders would not have been the same without my 224 office mates; James McCallum, Dylan Irvine, and (by *proxi*) Cameron Wood. Thanks for all the awesome homebrew, lunches, and Thursday beers.

I also want to thank my mum and dad for all the late night/early morning phone calls. Your support has been invaluable. I also want to mention all those outside of uni which have made my time in Adelaide all the more interesting and rewarding; Michelle and Matthew Sorell, Nic Rawlence, Jess Wadley, the Adelaide Bellringer, and last but not least Graham Gower.



# Summary

Quantifying the spatial variability of surface water-groundwater fluxes remains a challenge. The ability to either upscale point measurements or down scale reach/catchment scale measurement invariably introduces error into the estimation processes. This thesis addresses two methods that have been used to estimate surface water – groundwater flux, and investigates an approach to determining stream-aquifer connection state. The aims of this Doctoral thesis are to: 1) determine the representative scale at which standard hydraulic methods can be applied in this field of research, 2) quantify the variability in surface water – groundwater fluxes in ephemeral environments, and 3) develop methods of measuring hydraulic heads beneath and adjacent to streams.

In the first part of this research, the spatial scale of Darcy's law was investigated in the context of surface water – groundwater interaction. The primary supposition being that when applying Darcy's law to estimate groundwater discharge to a stream, the estimated discharge determined using a well at a distance of 50 m will encapsulate discharge over a greater proportion of the stream than a well at a distance of 10 m. This was investigated using numerical methods and stochastic  $K$ -fields to determine the influence of aquifer properties i.e., variance and correlation length of the  $K$ -fields on this question of scale. An estimate of the integrated hydraulic conductivity between the well and stream was determined by simulating a change in stream stage. The findings of this body of work suggest that an approximate 1:1 relationship exists between the distance of the observation well and the length of stream represented by the Darcian groundwater discharge estimate. In addition to this, the correlation length within the aquifer will strongly influence the variability in the discharge estimates. A similar approach was applied to a highly instrumented field site. The results of the field study concur with those of the numerical simulations i.e., variability in discharge estimates decreases as the distance of the well from the stream increases.

The second part focussed on determining the spatial variability in seepage flux beneath

an ephemeral channel. The use of flood front movement along a channel has emerged as a technique to determine the hydraulic conductivity of streambed sediments and thereby quantify the seepage flux for a given flow event. This approach was applied to a controlled flow event along a 1387 m reach of an artificial stream channel. We investigated the usefulness including surface water and groundwater data to assist in the calibration processes. The results of this study identified areas of high seepage fluxes in the upstream reaches and low seepage fluxes in the downstream reaches. A Latin Hypercube Monte Carlo analysis of the model indicated that specific yield had the strongest influence on the calibration.

The final part of this research investigated a well completion design which would enable the direct monitoring of the connection state of a stream, by enabling placement of wells beneath streams and floodplains. This approach required the well to be sealed so that surface water would be unable to enter, and the total pressure (from a non-vented pressure transducer) within the well could be monitored. A controlled laboratory experiment was used to compare the total pressure response in an open and sealed well to various water levels. The results indicated that the total pressure within the open and sealed wells were equal. Therefore, the groundwater response in the aquifer can be obtained using the total pressure data obtained from within a sealed well. The advantage of this approach is that it negates the need for tall standpipes and additional infrastructure, which would otherwise be damaged during high flow events.

# Chapter 1

## Introduction

### 1.1 Background

The past 30 years has seen the emergence of policy approaches that consider surface water and groundwater to be an integrated resource (Winter et al., 1998; Sophocleous, 2002). This has become increasingly important in areas where concerns for water availability have required consideration of long-term resource sustainability and the health of water-dependent ecosystems. Quantifying surface water –groundwater exchange fluxes has thus become a key focus of research to aid regional water planning and management (McCord et al., 1997; Eaton, 2006; Fleckenstein et al., 2006; Kalbus et al., 2008, 2009).

The spatial variability of surface water – groundwater exchange fluxes along a stream or river are a function of the geology and hydrogeology of the catchment (Toth, 1970). Nested within this larger scale are controls at a smaller scale, e.g., streambed permeability and channel geometry at the reach scale, and small scale streambed morphology such as pool-riffle sequences and gravel bars causing hyporheic exchange (Stonedahl et al., 2010). Streambed properties (e.g., hydraulic conductivity) also play a key role in determining the magnitude of the flux (Landon et al., 2001; Sanchez-Vila et al., 2006; Genereux et al., 2008). Variability in surface water – groundwater exchange fluxes will have an impact on the quality and the quantity of water available for use in agriculture, industry and domestic households (Sophocleous, 2002; Winter et al., 1998). The discharge of groundwater into rivers aids in sustaining base flow, controls water temperature, and facilitates nutrient transport, all of which influence the ecological processes within the surface water (Cook et al., 2006; Hatch et al., 2006; Gleeson et al., 2009; Kennedy et al., 2009; McCallum et al., 2012). Conversely, recharge from rivers into aquifers contributes to sustaining

groundwater resources, particularly in arid to semi-arid environments where rainfall is scarce and highly localised (Chenini and Ben Mammou, 2010; Jolly et al., 2008; Ragab and Prudhomme, 2002; Scanlon et al., 2006). However, this exchange is neither constant in space or in time, making it a challenge to quantify the surface water-groundwater exchange at scales appropriate for management.

Broadly, surface water – groundwater interactions can be divided into two categories; gaining (groundwater maintains base flow within the stream) and losing (stream water infiltrates through to the water table). The type of exchange will significantly alter the hydrological/hydrogeological processes (i.e., unsaturated flow versus saturated flow) and therefore the tools available to investigate them (Winter et al., 1998).

Kalbus et al. (2006) provides a review of the methods applied to quantify groundwater discharge to streams. A critical issue is the scale at which each of the different methods can be applied. For example, those methods applied to the surface water tend to provide a spatially integrated estimate of groundwater discharge over kilometres, i.e., hydrograph separation, stream flow gauging, and environmental tracers. As a result, it may be problematic if these estimates need to be down-scaled to provide information at a smaller scale (Blöschl, 2001; Cushman, 1986). Methods applied to the subsurface generally provide point scale aquifer information from which fluxes can be inferred i.e., hydraulic head and hydraulic gradient. Up-scaling this data will introduce errors into the estimation of groundwater discharge.

Similar challenges occur when estimating groundwater recharge from ephemeral and intermittent streams (Wood, 2009). Shanafield and Cook (in press) provide a comprehensive review of the common methods applied to estimate groundwater recharge in arid and semi-arid environments. In these environments, obtaining field data becomes problematic due to the unpredictability of flow events (Pilgrim et al., 1988). The most commonly used methods, such as temperature (Constantz, 2008) or soil moisture profiles (Dahan et al., 2007), provide data at the point scale. Surface geophysical methods can provide a more integrated estimate of streambed properties and cover a greater area (Wojnar et al., 2013; Pool and Eychaner, 1995), although are unable to give direct flux estimates.

At present, a significant disconnect exists between the scale of practical application

of field techniques for the characterisation of surface water – groundwater interactions, and the scale of information required for implementation in numerical models. Whilst there has been an increased focus on determining the impact of variability in aquifer properties upon surface water – groundwater exchange fluxes, there are still several areas requiring further research and investigation to enhance our ability to adequately quantify the available water resources. Key knowledge gaps include:

1. *the magnitude of spatial variability in surface water – groundwater interaction, particularly in losing streams*
2. *the impact of spatial variability on the methods applied to obtain estimates of surface water – groundwater exchange*

The most easily obtained data for assessing surface water – groundwater exchange is groundwater level and surface water level data. This provides knowledge of the hydraulics in the area of interest, which helps to establish the groundwater flow patterns (Freeze and Cherry, 1979). Groundwater level data provides insight into aquifer properties by responding when stresses such as pumping and recharge occur (Gomez-Hernandez and Gorelick, 1989; Butler, 1990; Scanlon et al., 2002; Coptý and Findikakis, 2004). Similarly, when groundwater data is coupled with surface water level data it can aid characterisation and estimation of the fluxes via the application of Darcy's law (Kalbus et al., 2006; Rosenberry and LaBaugh, 2008). Due to the availability of hydraulic data, this research has focussed on its inclusion, as the primary source of information, in the analysis of surface water – groundwater fluxes.

## **1.2 Research aims**

This doctoral research broadly addresses the impact of spatial variability in aquifer properties on the surface water – groundwater fluxes estimated via different methods applied. The themes covered in this thesis include the use of hydraulic methods and data in determining surface water – groundwater fluxes, the scale limitations on estimating surface water – groundwater fluxes in heterogeneous environments, the relative importance of different data types when estimating surface water – groundwater fluxes, and

the development of new tools for determining surface water – groundwater connection. Specifically, this body of work aims to:

1. *determine the representative scale at which standard hydraulic methods can be applied in this field of research,*
2. *quantify the variability in surface water – groundwater fluxes in ephemeral environments*
3. *develop methods of measuring hydraulic heads beneath and adjacent to streams.*

This thesis is comprised of an introduction, three stand-alone but related pieces of research work and conclusions. The introduction (Chapter 1) provides a brief overview of the key knowledge gaps and main issues in determining surface water – groundwater fluxes where significant spatial variability is present. The three research aims outlined above are addressed in three manuscripts and are contained in Chapters 2, 3, and 4 of this thesis. Each of these chapters can be read independently as a stand-alone piece of research, including introduction, methodology, results, discussion, and conclusion sections. Of the three manuscripts, one is currently in press and two are under review for publication in international hydrogeological journals. The conclusions and future directions suggested by this research are outlined in Chapter 5.

## Chapter 2

# The representative stream length for estimating surface water - groundwater exchange using Darcy's Law

Noorduijn, S. L., Harrington, G. A., and Cook, P. G. (2014) The representative stream length for estimating surface water - groundwater exchange using Darcy's Law, Journal of Hydrology, <http://dx.doi.org/10.1016/j.jhydrol.2014.03.062>



## 2.1 Abstract

Groundwater discharge to streams is spatially variable. We often estimate this flux based on an averaged measurement of hydraulic gradient and local estimate of hydraulic conductivity. It is important to understand how this estimated flux value relates to the flux into the stream. In this study we introduce the concept of representative stream length. The estimated flux value best represents the groundwater discharge over the representative stream length. We simulated groundwater discharge to a stream using synthetic stochastic hydraulic conductivity fields to investigate the impact of heterogeneity (variance and correlation length) on the estimated groundwater discharge and the representative stream length of this discharge. To obtain estimates of hydraulic conductivity between the stream and piezometer, the groundwater head response to a known change in stream stage was simulated and analyzed using a well-known analytical solution. The results of the theoretical investigation showed that the representative stream length of the groundwater discharge estimate was approximately equal to the distance of the piezometer from the stream, that is, groundwater discharge estimated using Darcy's law from a piezometer 50 m from a stream will approximately represent the discharge occurring over a 50 m length of the stream. Furthermore, the results suggest that the variability in the estimated groundwater discharge significantly reduced when the distance of the piezometer from the stream increased. A field experiment was conducted using two controlled stream-stage change tests and found that results were consistent with the theoretical experiment. That is, as the distance of the piezometer from the stream increased, the variability in discharge estimates reduced. The implication of this finding is that future studies estimating groundwater discharge to streams applying Darcy's law need to consider the representative stream length, as this will impact the spatial scale over which the discharge estimate can be applied.

## 2.2 Introduction

Darcy's law is widely applied to estimate surface water – groundwater exchange flux (Darcy, 1856; Kalbus et al., 2006; Parsons et al., 2008). This method relies on estimates

of both the aquifer hydraulic conductivity and the hydraulic gradient. In practice, heterogeneity within the aquifer will mean that both hydraulic conductivity and hydraulic gradient will be spatially variable (Sanchez-Vila et al., 2006). The flux to the stream will also be spatially variable. In practice, Darcy's law is applied using point measurements of hydraulic head and local measurements of hydraulic conductivity. We therefore need to understand how the calculated flux relates to discharge along the stream. Conceptually, as the distance of the piezometer from the stream increases, the discharge estimate will be representative of a longer stream length. We define this stream length as the "representative stream length" which is analogous to the representative elementary volume described in most hydrogeology texts (Bear, 1972; ?). Understanding the relationship between the distance of the piezometer from the stream, the aquifer heterogeneity, and the representative stream length is important for upscaling (Millham and Howes, 1995).

One method used to determine hydraulic conductivity near streams is using groundwater level response to stream stage change (Rorabaugh, 1964; Hall and Moench, 1972; Moench and Barlow, 2000; Hantush, 2005; Koussis et al., 2007). An advantage of this method over pumping tests is that the hydraulic conductivity is measured between the stream and piezometer, therefore at a more appropriate scale (Butler, 1990; Rötting et al., 2006; Yeh et al., 2007, 2009). The effect of aquifer heterogeneity is incorporated in the pressure response observed in the piezometer (Millham and Howes, 1995; Serrano et al., 2007; Spanoudaki et al., 2010).

Here we examine how representative stream length varies with the distance of the piezometer from the stream and the magnitude of aquifer heterogeneity. A numerical approach was used to compare the spatial variation in groundwater discharge into a stream (per unit length of stream) with the estimated groundwater discharge rate obtained using Darcy's law. We subsequently apply this approach to a highly-instrumented field site to determine the scale of aquifer heterogeneity and obtain estimates of hydraulic conductivity and groundwater discharge.

## 2.3 Numerical simulations

Numerical simulations were conducted to determine how representative the Darcy's law groundwater discharge estimate was of the actual discharge occurring along the stream. Varying both the aquifer heterogeneity and location of the piezometers (used in the Darcy's law discharge calculation) allowed a relationship to be established between the distance of the piezometer from the stream and the representative stream length of the discharge estimate. The overall approach was as follows: 1) generate a series of synthetic aquifers to represent different levels of heterogeneity; 2) set up a suite of groundwater models based on these synthetic aquifers to simulate groundwater flow towards a gaining stream; this provided both the steady state hydraulic heads (and steady state gradient) and the actual numerical groundwater discharge flux along the stream (obtained from the water balance). 3) Compare groundwater discharge flux obtained from the model water balance to Darcy's law groundwater discharge estimates. In order to obtain the steady state Darcy's law groundwater discharge, an estimate of the hydraulic conductivity was required. This was obtained by analyzing the groundwater head responses in piezometers at various distances from the stream, to a change in stream stage.

Table 2.1: Description of model parameters.

Parameter		Units
$K$	Hydraulic conductivity	$\text{m d}^{-1}$
$\tau$	Correlation Length	m
$\sigma^2$	Variance	-
$y$	Distance parallel to the stream	m
$x$	Distance perpendicular to the stream (obs. well distance)	m
$t$	Time	d
$h(x, t)$	Groundwater head at location $x$ and time $t$	m
$\alpha$	Aquifer diffusivity	$\text{m}^2\text{d}^{-1}$
$T$	Aquifer transmissivity	$\text{m}^2\text{d}^{-1}$
$S$	Aquifer storage coefficient	-
$K_{eff}$	Effective hydraulic conductivity	$\text{m d}^{-1}$
$Q_{eff}^{x,y}$	Darcy's law groundwater discharge calculated using $K_{eff}$	$\text{m}^3 \text{d}^{-1} \text{m}^{-1}$
$Q^y$	Numerical groundwater discharge from the MODFLOW model	$\text{m}^3 \text{d}^{-1} \text{m}^{-1}$
$\overline{Q^y}$	Average groundwater discharge from the MODFLOW model over stream length $l$	$\text{m}^3 \text{d}^{-1} \text{m}^{-1}$

### 2.3.1 Model conceptualization and set up

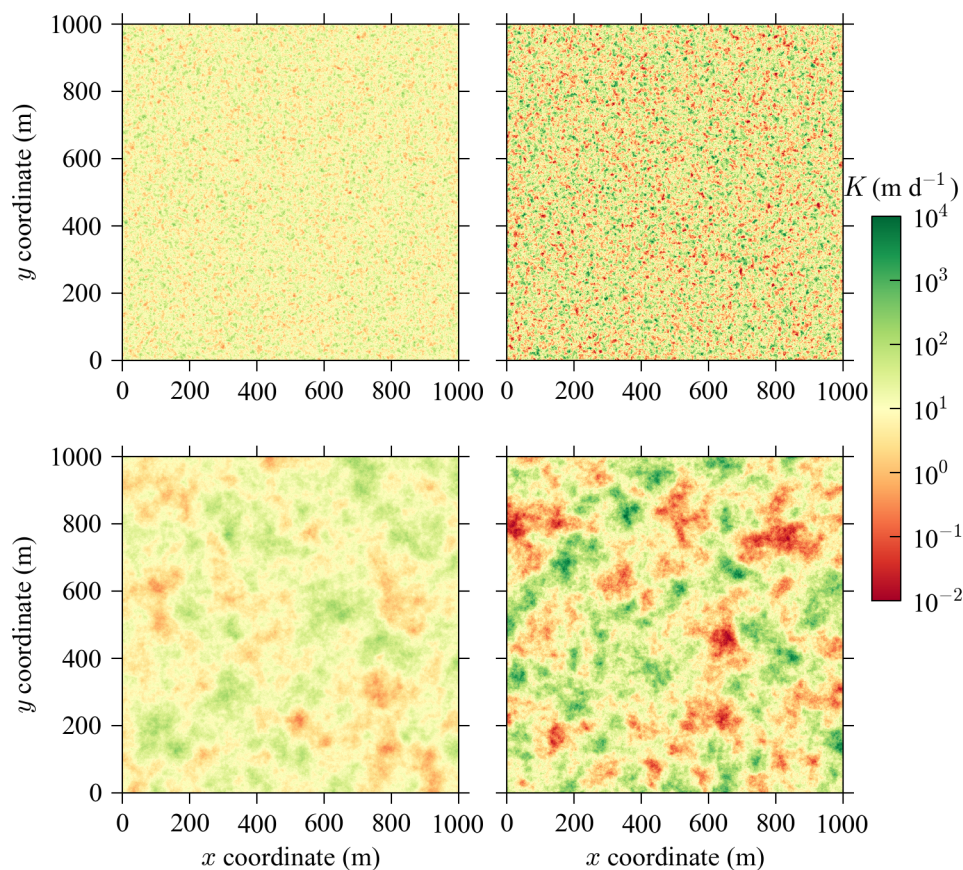


Figure 2.1: Examples of the synthetically generated  $K$  fields with different variances ( $\sigma^2$ ) and correlation length ( $\tau$ ). (a)  $\sigma^2 = 1.0$  and  $\tau = 10$  m, (b)  $\sigma^2 = 4.5$  and  $\tau = 10$  m, (c)  $\sigma^2 = 1.0$  and  $\tau = 100$  m, and (d)  $\sigma^2 = 4.5$  and  $\tau = 100$  m.

#### 2.3.1.1 Synthetic aquifers

The Sequential Gaussian Simulation (SGSIM) method from the Geostatistical Software Library (GSLIB) (Deutsch and Journel, 1998) was used to generate random, isotropic, log-normally distributed, 2D hydraulic conductivity ( $K$ ) fields. The model domain was 1000 m by 1000 m with a uniform 1 m by 1 m cell size. All  $K$  fields were based on a spherical variogram with an isotropic correlation length of  $\tau_x = \tau_y = \tau$ , where  $\tau$  was 10, 50, 100, and 200 m. The geometric mean of the  $K$  values was  $10 \text{ m d}^{-1}$  (natural logarithmic mean was 2.3). The degree of heterogeneity was controlled by the variance ( $\sigma^2$ ) of the  $\ln(K)$  field, values of  $1.0 \text{ m}^2 \text{d}^{-2}$  and  $4.5 \text{ m}^2 \text{d}^{-2}$  were chosen to represent a lower

and higher level of  $\ln(K)$  variability respectively. Thirty realizations of the randomly correlated hydraulic conductivity fields were generated for each  $\tau$  and  $\sigma^2$  combination. Four examples of the synthetic hydraulic conductivity fields are shown in Figure 2.1.

It must be noted that the limitations of this approach are that the  $K$  field is isotropic and stationary. In addition to this, an important limitation of the use of multi-Gaussian models is that the level of connectivity between structures is purely random and tend to a more gradual change in hydraulic conductivity values. In the real world alluvial setting, the variability within the aquifer tends towards more discrete changes in  $K$  and more structural heterogeneity (Fleckenstein and Fogg, 2008; Fleckenstein et al., 2006; Conant Jr, 2004). Also, field-scale correlation length ranges from several meters (MADE site (Barlebo et al., 2004)) to kilometers (Hoeksema and Kitanidis, 1985). However, the practicalities of simulating flow within heterogeneous fields in a numerical model are a challenge therefore the model correlation length is limited to  $\tau = 200$  m.

### 2.3.1.2 Model Design

Groundwater flow through the synthetic aquifer to a 1000 m long, straight stream was simulated using MODFLOW-NWT (Harbaugh, 2005; Niswonger et al., 2011). The streambed was assumed to be directly incized into the aquifer such that the streambed  $K$  was equal to that of the aquifer. A schematic diagram of the model domain is shown in Figure 2.2(a), refer to Table 2.1 for parameter descriptions. The constant head boundary ( $x = 1000$  m) represents the regional groundwater level ( $h_2 = 9.0$  m) and the time variant head boundary ( $x = 0$  m) represents the fully penetrating stream ( $h_1(t_0) = 8.5$  m). The lateral boundaries ( $y = 0$  m and 1000 m) and the bottom boundary (base of the aquifer) are no flow. The specific yield was set to 0.2, and did not vary spatially. Under steady state conditions the mean hydraulic gradient is  $0.0005$  ( $\text{m m}^{-1}$ ). Piezometers (implemented in MODFLOW as observation wells) were placed at 20 m spacing parallel to the stream and a buffer zone of 100 m was allowed to minimize the impact of the lateral no flow boundaries on the stream length analysis (total number of piezometers for each line parallel to the stream was 41). The spacing of the piezometers perpendicular to the stream was 2 m from a distance of 2-20 m, 10 m from a distance of 20-70 m, 25 m from a distance of

100-300 m and 50 m from a distance of 300-350 m. A total of 1025 piezometers were located in the model. The distance of the piezometer from the stream will henceforth be referred to as the piezometer distance.

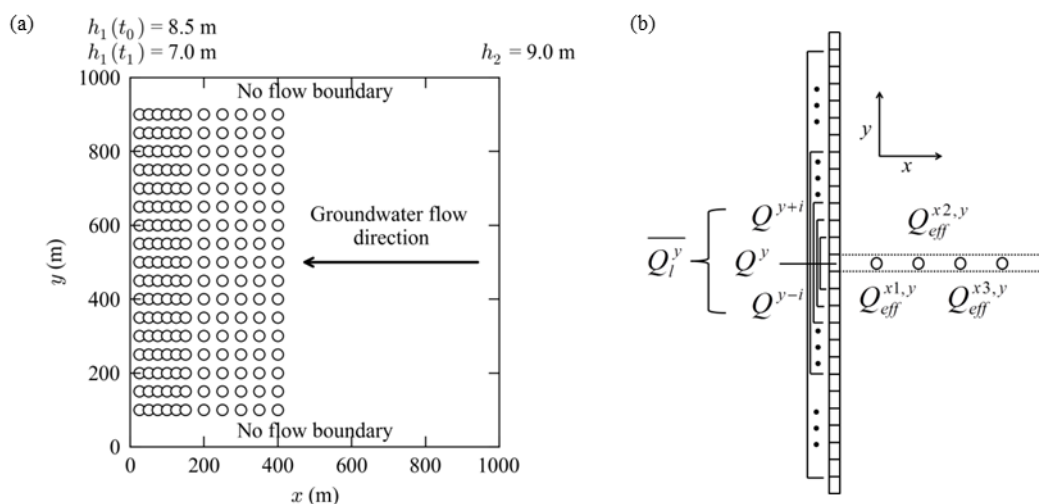


Figure 2.2: (a) Schematic of the model set up and location of the observation wells (unfilled circles). Constant head boundary on the right ( $h_2=9.0$  m) and a time variant head boundary on the left which represents the stream ( $h_1(t_0)=8.5$  m,  $h_1(t_1)=7.0$  m). (b) shows how the discharge estimates derived from the analytical solution are related to the modeled stream discharge from the MODFLOW model. For clarity, only a selected number of length are shown. Refer to section 2.2.1.3, Eq. 2.1 and Table 2.1 for parameter descriptions.

### 2.3.1.3 Steady state groundwater discharge

The model was run to steady state, and the steady state ( $SS$ ) groundwater discharge for each grid cell along the stream was obtained from the model water balance (hereafter denoted as  $Q^y$ ; Table 2.1). The variability in the groundwater discharge along the stream will reflect the variability in the hydraulic conductivity of the aquifer. These grid-scale groundwater discharge values form the basis of the comparison with Darcy's law groundwater discharge estimates calculated from each of the piezometers in the numerical model. The latter were calculated using the head difference between the piezometer and stream, and an estimate of the hydraulic conductivity as described in the next section (section 2.3.1.4).

The aim of comparing groundwater discharge along the stream with Darcy's law

groundwater discharge calculated for each of the piezometers was to determine a relationship between the piezometer distance and the representative stream length. The general supposition was that if the piezometer was further from the stream, then the estimated discharge rate would represent groundwater discharge over a longer reach of the stream. The following steps were taken for each aquifer realization.

The steady state numerical groundwater discharge for each cell along the stream ( $Q^y$ ) was used to calculate the average numerical groundwater discharge ( $\overline{Q}_l^y$ ) for stream lengths of 1 - 201 m centered at the same y-coordinate as the piezometer (Figure 2.2(b)). The following equation describes the method used:

$$\overline{Q}_l^y = \frac{1}{l} \sum_{i=-(l-1)/2}^{(l-1)/2} Q^{y+1} \quad l = 1, 3, 5, \dots, 201 \quad (2.1)$$

where  $\overline{Q}_l^y$  is the length averaged  $Q^y$  ( $L^3T^{-1}L^{-1}$ ) centered around  $y$ , where  $y$  is the position of the piezometer along the stream, and  $l$  is the total number of cells (or length for a 1 m cell width) ( $L$ ). The maximum length considered in this study was limited to 201 m as this was the maximum length possible without intercepting the no flow boundaries..

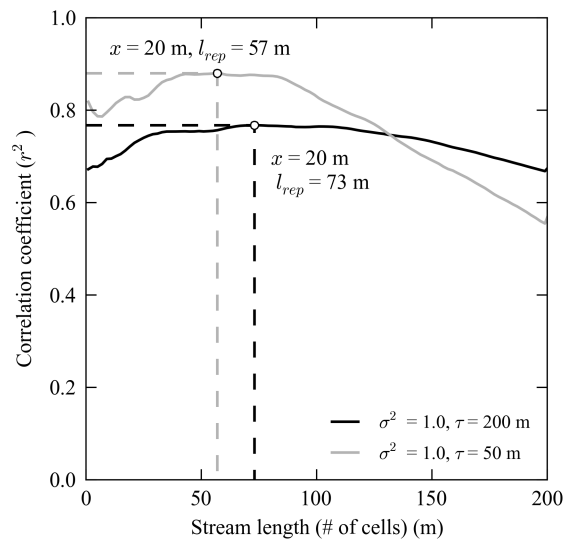


Figure 2.3: Examples of the distribution of the correlation coefficient between  $Q_{eff}^{x,y}$  and  $Q_l^y$  for different equivalent stream discharge length ( $l_{equ}$ ) (m).

For a given distance from the stream,  $x$ , the equivalent stream discharge length ( $l_{equ}$ )

was determined as the highest correlation coefficient ( $r^2$ ) between  $Q_{eff}^{x,y}$  (for all wells at a given distance from the stream) and for length from 1 m to 201 m (e.g., Figure 2.3). For example, for one realization the Darcy's law groundwater discharge ( $Q_{eff}^{x,y}$ ) for all observation wells at  $x = 20$  m are considered. The  $r^2$  was then determined between the forty one estimated  $Q_{eff}^{x,y}$  (i.e., number of observation wells parallel to the stream) at  $x = 20$  m and the forty one length averaged numerical groundwater discharge ( $\overline{Q}_l^y$ ) for  $l = 1, 3, 5, 7, 9 \dots 201$  m. All  $Q_{eff}^{x,y}$  and  $\overline{Q}_l^y$  pairs were located at, or centered on, the  $y$  coordinate. In principal, the highest  $r^2$  value indicated the length of stream encapsulated by the Darcy's law groundwater discharge estimate at  $x = 20$  m, based on its ability to predict the averaged numerical groundwater discharge. The stream length ( $l$ ) for each of the thirty realizations was used to determine the average  $l_{rep}$  and this was repeated for all  $\tau$  and  $\sigma^2$  aquifer combinations.

#### 2.3.1.4 Stream stage response to estimate $K_{eff}$ and $Q_{eff}$

The effective hydraulic conductivity ( $K_{eff}$ ) between the observation well and the stream was determined using a step decline in stream stage of 1.5 m ( $h_1(t_1) = 7.0$  m), simulated at the time varying head boundary ( $x = 0$ , Figure 2.2(a)). This transient state simulation was run for 20 days with a time step of 0.01 days. The groundwater response at each of the observation wells was exported for each  $K$  field simulated.

Inverse modeling with the Hall and Moench (1972) analytical model were used to determine the effective hydraulic conductivity ( $K_{eff}$ ) between the stream and observation well. The analytical model uses the process of convolution of an input function (i.e., stream stage from the numerical model) to calculate the head response at a distance  $x$  (L) from the stream (observation well distance) based on a unit step response of the system:

$$h(x,t) = \int_0^t F'(v)P(x,t-v)dv \quad (2.2)$$

where  $h(x,t)$  is the groundwater head relative to a zero datum (L),  $F'(v)$  is the rate of change of the system input; for this work  $F'(v)$  was the rate of change in stream stage

$(h_s)$  ( $LT^{-1}$ ),  $P(x,t)$  is the unit step response of the system (-) and

$$F'(t) = \frac{h_s(t) - h_s(t-1)}{\Delta t} \quad (2.3)$$

$$P(x,t) = \text{erfc} \left( \frac{x}{(4\alpha t)^{0.5}} \right) \quad (2.4)$$

where  $\text{erfc}$  is the complimentary error function,  $x$  is the observation well distance,  $\alpha$  is the aquifer diffusivity ( $T/S$ ) ( $L^2T^{-1}$ ),  $S$  is the aquifer storage coefficient (-),  $T$  is aquifer transmissivity ( $L^2T^{-1}$ ), and  $t$  is time (T). The analytical model assumptions are based on the linearized Boussinesq equation; that is, the stream is fully penetrating, the aquifer is semi-infinite and transmissivity is constant.

The aquifer diffusivity was estimated using PEST (Doherty, 2010), which uses the least squares fitting routine and Gauss Marquardt Levenburg method to minimize the objective function:

$$\phi = \sum_{k=1}^{N_{obs}} (h_k^m - h_k^s)^2 \quad (2.5)$$

where  $\phi$  is the objective function value (-),  $N_{obs}$  is the total number of head observations (-),  $h^m$  is the head response generated at each observation well in the MODFLOW model (L), and  $h^s$  is the simulated head response using the analytical model (L). Only aquifer diffusivity ( $\alpha = T/S$ ) was allowed to vary during the calibration processes.  $K_{eff}$  was then calculated by:

$$K_{eff} = \frac{\alpha S}{b} \quad (2.6)$$

where  $S$  is the specific yield of the aquifer and  $b$  is the aquifer thickness of the MODFLOW model, which were 0.2 and 10 m respectively.

Steady state groundwater discharge was then estimated using Darcy's law; that is, the product of the steady state hydraulic gradient derived from the MODFLOW model, the estimated  $K_{eff}$  from the Hall and Moench (1972) analytical model, the cell width (1 m) and the initial saturated aquifer thickness. This was repeated for all observation wells for each aquifer realization. All future reference to steady state groundwater discharge determined by this method is termed Darcy's law groundwater discharge ( $Q_{eff}^{x,y}$ ).

## 2.3.2 Model Results

### 2.3.2.1 Variability in $Q_{eff}$ versus piezometer distance

In a heterogeneous aquifer, the aquifer spatial structure (represented by its correlation length and variance,  $\tau$  and  $\sigma^2$ ) will influence the variability in Darcy's law discharge estimates. Longer flow path length will reduce the influence of the variability in  $K$  resulting in an averaging of the estimated groundwater discharge. This is clearly visible in Figure 2.4, where the range of groundwater discharge estimates decreases as the distance to the stream increases.

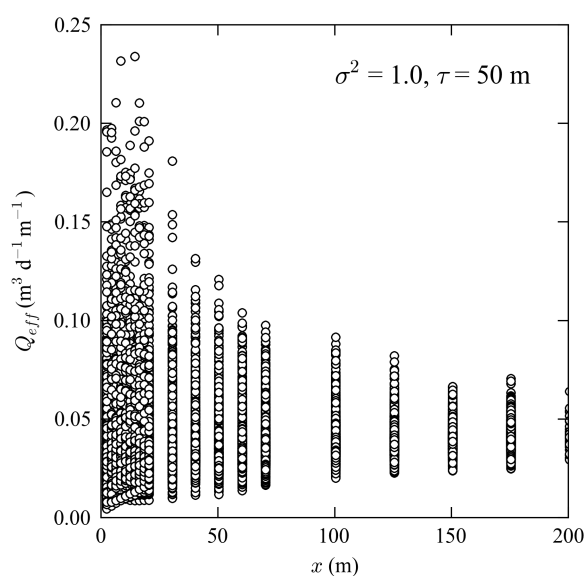


Figure 2.4: The spread in groundwater discharge estimates related to the observation well distance for 30 aquifer realizations with a variance = 1.0 and correlation length = 50 m.

The variability in effective groundwater discharge for each value of  $x$  can be expressed using the coefficient of variation (standard deviation normalized by the mean),  $CV(Q_{eff}^x)$ . The relationship between the piezometer distance and  $CV(Q_{eff}^x)$  is shown for different correlation lengths and variances in  $\ln(K)$  in Figure 2.5. The results indicate that as the piezometer distance increases, the variability in discharge estimates decreases. This suggests that the influence of low or high  $K$  zones diminishes as the piezometer distance increases, and as a result the estimated discharge rate will approach the mean discharge value.

The  $CV(Q_{eff}^x)$  decreases rapidly with increasing  $x$  for  $\tau = 10$  m, but decreases at a much

lower rate for  $\tau = 50 - 200$  m. Where  $x \geq 100$  m,  $CV(Q_{eff}^x)$  increases with increasing correlation length. This suggests that where there are large correlation lengths within an aquifer (i.e., distance between two similar  $K$  zones  $> 100$  m), greater distances between the piezometer and stream are needed to obtain reliable estimates of the mean discharge rate. Variance of the underlying  $K$  field of the aquifer influences the magnitude of the  $CV(Q_{eff}^x)$  and the rate at which it diminishes, e.g., for  $\tau = 10$  m the  $CV(Q_{eff}^x)$  stabilizes beyond  $x = 150$  m for  $\sigma^2 = 1.0$  and  $x = 250$  m for  $\sigma^2 = 4.5$ . The difference in magnitude of  $CV(Q_{eff}^x)$  is clearly visible when comparing  $\sigma^2 = 1.0$  and  $4.5$  (Figure 2.5). If an infinite model domain were used, the  $CV(Q_{eff}^x)$  close to the stream should be equal for all correlation lengths if the variance is the same. However, this is not the case, and may be a function of numerical error, number of realizations, and the limited extent of the model domain.

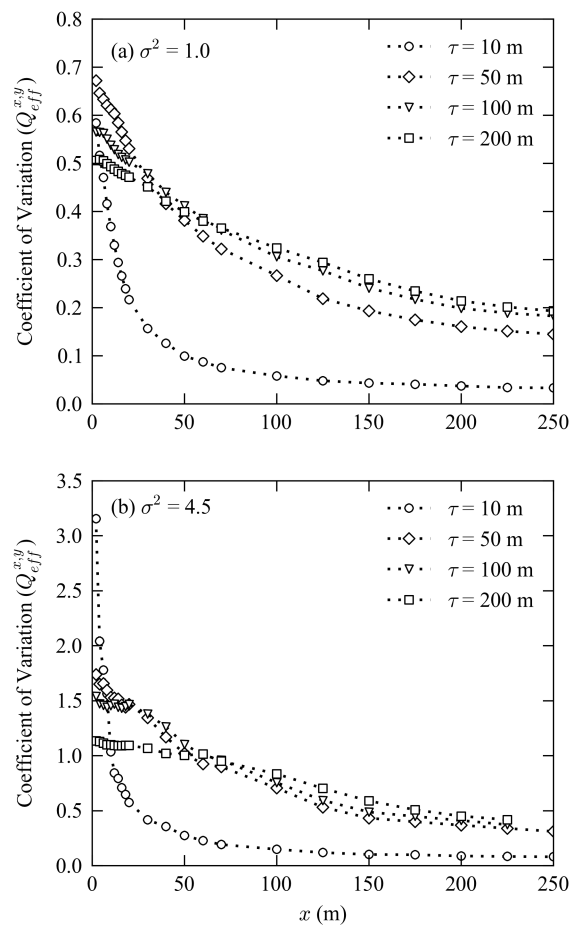


Figure 2.5: Variability in the Darcy's law groundwater discharge ( $CV(Q_{eff}^{x,y})$ ) as a function of the observation well distance for two different  $\ln(K)$  variances.

Figure 2.6 shows the  $CV(Q_{eff}^x)$  relative to the piezometer distance normalized by the

correlation length ( $x/\tau$ ), i.e., the number of correlation lengths within the aquifer between the stream and piezometer. For both variances, Figure 2.6 indicates that for any given  $x/\tau$  ratio the  $CV(Q_{eff}^x)$  is lowest for the longer correlation length. The influence of the variance amplifies the difference between the trends of the correlation lengths, i.e., where  $x/\tau = 1.0$ , the difference between  $\tau = 50$  m and 200 m for  $\sigma^2 = 1.0$  is 0.2 and for  $\sigma^2 = 4.5$  it is 1.2.

It might be expected that the relationship between  $CV(Q_{eff}^x)$  and  $x/\tau$  would be independent of correlation length. This relationship would give an indication of the required number of correlation lengths needed to obtain a reliable estimate of groundwater discharge. Results indicate that the relationships between  $CV(Q_{eff}^x)$  and  $x/\tau$  appear to converge after 2.5 correlation lengths ( $x/\tau > 2.5$ ). The value of  $CV(Q_{eff}^x)$  is lower at this point for  $\sigma^2 = 1.0$  than for  $\sigma^2 = 4.5$ .

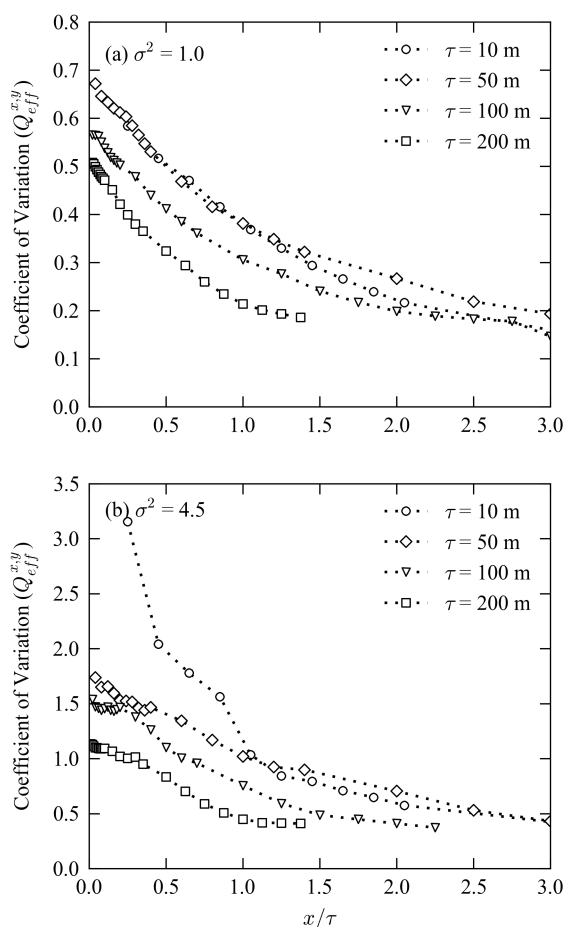


Figure 2.6: Darcy's law groundwater discharge variability ( $CV(Q_{eff}^{x,y})$ ) as a function of the ratio of the observation well distance to the correlation length ( $x/\tau$ ), shown for two different  $\ln(K)$  variances.

### 2.3.2.2 Comparison of measurement scales

The effective groundwater discharge ( $Q_{eff}^{x,y}$ ) and the numerical groundwater discharge ( $Q^y$ ) were compared to define the representative stream length. For some of the realizations the maximum  $r^2$  values were much more easily defined peaks, whereas other realizations displayed a plateau in  $r^2$  values (Figure 2.3). For all realizations, the range of  $r^2$  values used to determine equivalent stream discharge lengths were 0.30 - 0.99; the average across all realizations was  $r^2 = 0.7$ .

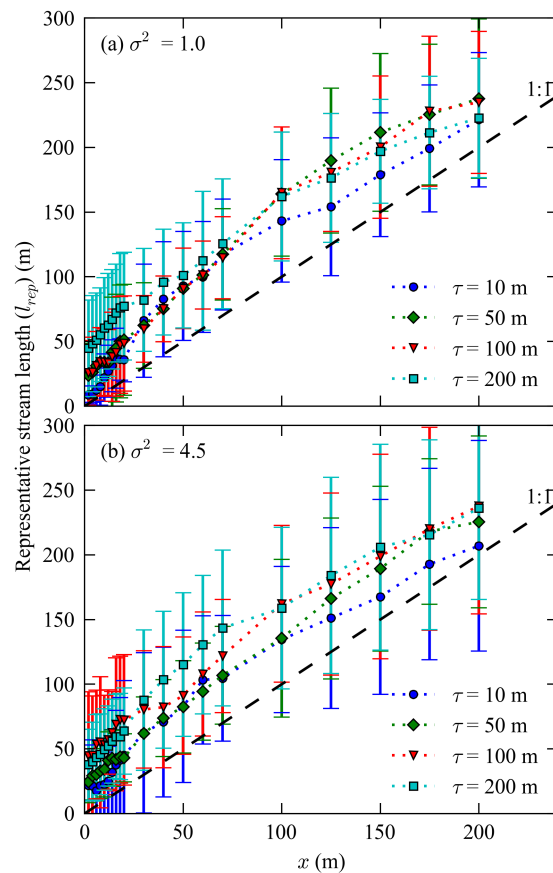


Figure 2.7: Changes in the estimated representative stream discharge length as a function of the observation well distance based on Darcy's law groundwater discharge ( $Q_{eff}^{x,y}$ ) and numerical groundwater discharge ( $Q^y$ ), (a) for an aquifer with  $\sigma^2 = 1.0$  and (b)  $\sigma^2 = 4.5$ . The error bars are the standards deviation in the equivalent stream discharge length for the 30 realizations.

The relationship between piezometer distance and representative stream length for the heterogeneous aquifers is shown in Figure 2.7. For both aquifer K variances, the representative stream lengths are approximately 50 m greater than the distance of the piezometer from the stream, but this difference is not significant when considering the

error bars. These results suggest that neither the variance nor correlation length within the aquifer has a marked effect on the representative stream length.

## 2.4 Example of field application

A similar methodology as described in the numerical simulations was applied to a field site. The aim was to determine whether comparable trends could be observed in a real world setting.

### 2.4.1 Field setting

A field experiment was performed on a reach of the Fairview Drain, an artificial and un-lined groundwater interception channel located in the South East of South Australia (lat.  $36^{\circ}43'22''$  long.  $140^{\circ}08'01''$ , 19.1 m Australia Height Datum AHD)). The Fairview Drain forms part of a system of channels constructed to lower the regional water table and mitigate the effects of dryland salinity, thereby enabling the land to be used for agriculture. The channel has a trapezoidal cross-section, approximately 2 m deep (thalweg approx. 17.3 m AHD) and 4 m wide, with  $33^{\circ}$  banks. No defined streambed exists within the drain and the bed slope along the experimental reach is  $0.00015$  ( $\text{m m}^{-1}$ ). The geology in close proximity to the field site consists of unconsolidated sandy clay/calcarene sediments which extend to a depth of 8 m below ground surface. These are underlain by unconsolidated bioclastic aeolianite deposits (the Padthaway Formation, 8 - 20 m bgl) and Narrawaturk glauconitic marl which acts as an aquitard ( $> 20$  m bgl) (Ward, 1974; Waterhouse et al., 1977). The channel is directly incised into the aquifer materials. The regional groundwater flow direction is north-westward and water table depth at the site is approximately 1.5 m below ground level (bgl). A number of flow regulators (i.e., weirs and gates) were constructed along the channel to allow water to be diverted or help maintain the water table at a specified level during the summer month. Twenty-nine monitoring wells were installed at the site; all are similarly constructed to a depth of 3.5 m bgl with a 2 m slotted section at the base (Figure 2.8).

Two stream stage experiments were conducted at the site: 10 Oct 2011, and 15 Oct 2012. For both experiments the flow regulator located downstream was completely

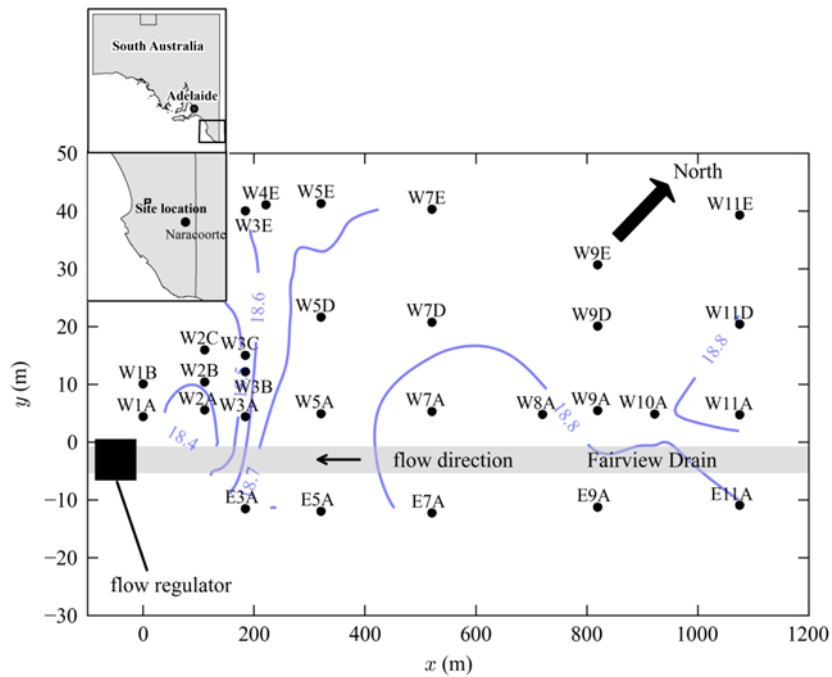


Figure 2.8: Map of the Fairview Drain experimental site showing the Fairview Drain, the location and ID for all observation wells (circles), location of the flow regulator, and the steady state groundwater contours (blue) in m AHD.

closed for 2 weeks prior to the experiment to allow the surrounding water table to come into equilibrium with the elevated stage within the stream. The flow regulator was then opened for 2 weeks; the stream stage dropped by 0.8 m during both experiments. Pressure transducers were installed in 21 piezometers for the first experiment, and 26 for the second experiment to monitor the groundwater level at 10 minute intervals (In-Situ Inc LevelTROLL® 300 Series,  $\pm 0.2\%$  accuracy, and In-Situ Inc. BaroTROLL®,  $\pm 0.05\%$  accuracy). Stream stage was monitored for both experiments at up-stream and down-stream locations.

## 2.4.2 Calculation of $K_{eff}$

Due to the distance of the observation wells from the stream ( $< 50$  m) and partial penetration of the stream into the aquifer, the analytical model of Hall and Moench (1972) was not appropriate for the analysis of the field data (ref. Appendix A). Partial penetration of the stream varied from 5-10% based on the depth to the Narrawaturk marl (aquitard), obtained from drilling logs for wells in the vicinity of the site. Accordingly, the field data was analyzed using a 2-dimensional homogenous MODFLOW model. The model is a

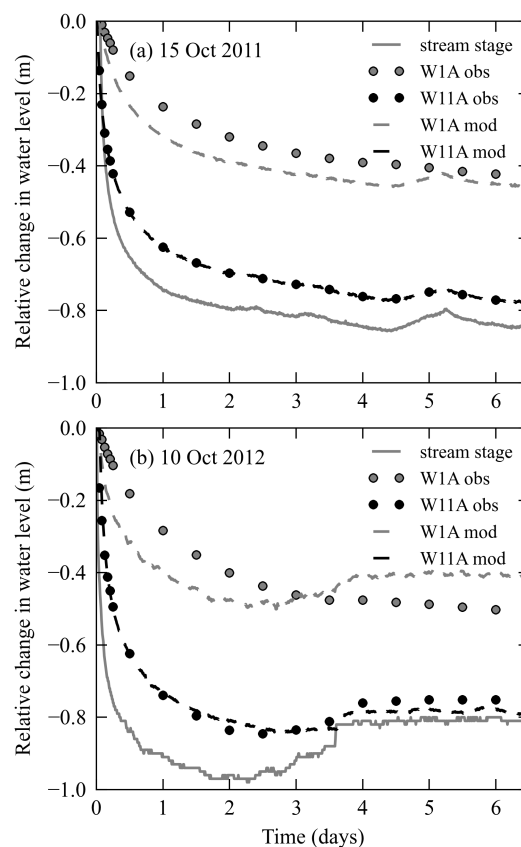


Figure 2.9: Calibration of the observation well data using MODFLOW (assuming 10% stream penetration) and PEST for the stage change experiments on (a) 15 Oct 2011 and (b) on 10 Oct 2012 respectively. The stream stage (solid gray line), the observed (circles) and the calibrated MODFLOW modeling fit (dashed line) are presented. Examples of both the best and worst calibration fits for the observation data are shown. For clarity, only two locations and part of the measured data points are shown.

20 m vertical slice of the aquifer perpendicular to the channel; top of the Narrawaturk marl assumed to be the base of the aquifer. Groundwater discharge into the channel was assumed to be symmetrical, therefore only half of the channel was modeled, with a vertical no-flow boundary beneath the stream and a horizontal no-flow boundary along the base of the model. A time varying specified head boundary was used to simulate the channel stage in the top model layer. A constant head boundary, 1000 m from the stream, was used to represent the regional groundwater flow.

PEST was used to optimize the  $K$  in the homogenous MODFLOW model using the stream stage and observation well hydrograph to constrain the calibration process. This allowed estimation of the  $K_{eff}$  for each observation well. Three distance groups were used to investigate the spatial relationship in estimated  $K_{eff}$ ;  $x < 6$  m,  $6 \text{ m} < x < 20$  m, and

20 m <  $x$  < 40 m.

### 2.4.3 Variability in estimated $K_{eff}$ and $Q_{eff}$

The ability of the numerical model to fit the observed groundwater response data was better in the wells furthest from the flow regulator (> 200 m upstream of the flow regulator). Examples of the groundwater response close to (e.g., W1A) and far from the flow regulator (e.g., W11A) are shown in Figure 2.9. The initial groundwater level in these wells was lower relative to the stream stage due to groundwater flowing around the flow regulator. Therefore the stresses on the system provided by the stream stage change were not fully realized in those wells less than 200 m from the regulator, thereby resulting in a poor calibration. From this point on, those wells with a poor calibration due to the presence of the flow regulator are excluded.

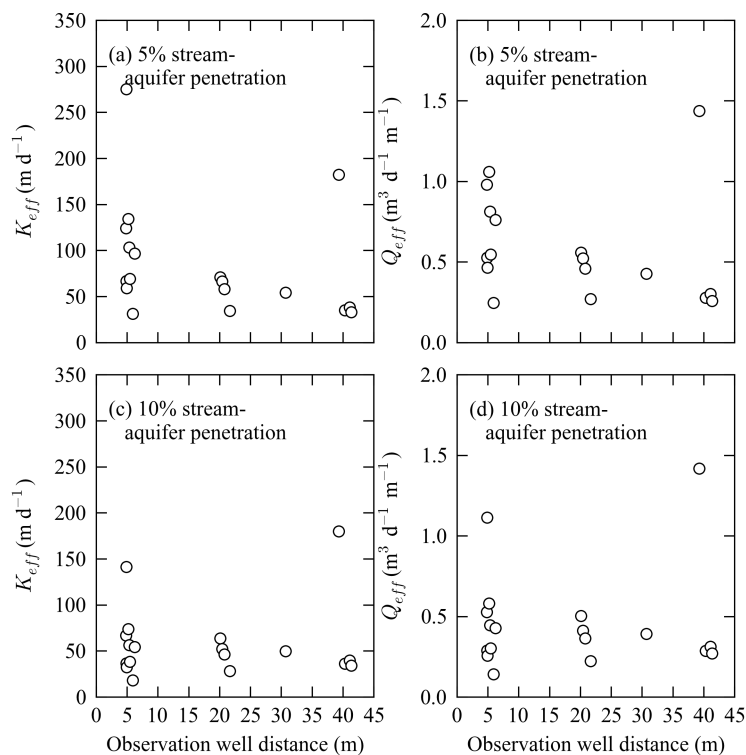


Figure 2.10: Influence of stream-aquifer penetration (5% and 10%) on the calibrated effective hydraulic conductivity ( $K_{eff}$ ) and steady state groundwater discharge ( $Q_{eff}$ ) as a function of the observation well distance.  $K_{eff}$  represent the geometric mean of the  $K_{eff}$  for each observation well determined from the MODFLOW model for both stage change experiments at the Fairview Drain experimental site.

The largest variation in estimated  $K_{eff}$  (and thus  $Q_{eff}$ ) at the Fairview Drain experimental site is observed for those observation wells closest to the stream (< 6 m), regardless

of whether a partial penetration of 5% or 10% is assumed (Figure 2.10). In general, the magnitude of this variation decreases as the distance between the well and stream ( $x$ ) increases, particularly for wells  $> 40$  m from the stream. The geometric mean and variance in the  $K_{eff}$  for the Fairview Drain experimental site are described in Table 2.2. This trend is consistent with the findings from the theoretical study where the variability in  $Q_{eff}^{x,y}$  decreased as observation well distance increased. One exception to this is the results obtained for observation well W11E, where  $x$  is 39.31 m and has an estimated  $K_{eff}$  of  $180 \text{ m d}^{-1}$  for both a 5% and 10% stream-aquifer penetration. All wells in transect 11 (E11A, W11A, W11D, and W11E in Figure 2.8) exhibit a higher than average estimated  $K_{eff}$  within their distance groups (i.e.,  $x < 6$  m,  $6 \text{ m} < x < 20$  m, and  $20 \text{ m} < x < 40$  m). This may be indicative of preferential flow path or high  $K$  zones within the aquifer, not intercepted at the other well locations. The influence of observation well W11E on the distribution of estimated  $K_{eff}$  at  $20 \text{ m} < x < 40$  m from the stream may decrease if more observation wells were present.

Table 2.2: Statistics for the estimated  $K_{eff}$  from the Fairview Drain experimental site (excluding transect 11 data).

	Distance (m)	Stream-aquifer penetration	
		5%	10%
Geometric mean $K_{eff}$ ( $\text{m d}^{-1}$ )	All	77.2	52.6
	0-6 m	94.3	51.8
	6-20 m	55.9	45.8
	20-40 m	38.4	38.9
Variance $\ln(K_{eff})$	All	0.447	0.375
	0-6 m	0.405	0.375
	6-20 m	0.069	0.075
	20-40 m	0.05	0.037

## 2.5 Discussion

Theoretical investigation has shown a linear relationship between the scale at which groundwater discharge to a stream is measured using Darcy's Law and the scale of groundwater discharge along the stream. While there are many other methods (i.e., besides Darcy's law) for estimating groundwater discharge to streams, many are limited to point

or reach scales (Kalbus et al., 2006), which is not always appropriate for groundwater management at the catchment or regional scale. This investigation has shown that when a well is approximately 50 m from the stream, the estimated groundwater discharge to the stream using Darcy's law only represents discharge over a stream length of 50 m. As the distance from the stream increases, more of the stream is captured in the discharge estimate. However at larger distances away from the stream the influence of other factors, e.g., pumping and evapotranspiration, also affect the gradient and water table response, which will impact the interpretation of the flux calculated by Darcy's law. Stream geometry (i.e., bank slope) will also influence the rate of groundwater and timing of groundwater discharge into a stream (Doble et al., 2012). Nevertheless, the value in this approach is that it provides a good initial estimate of exchange fluxes, particularly where data is sparse (e.g., Parsons et al. (2008)).

The statistical properties of the aquifer (variance and correlation length in  $K$  field) have only a minor impact on the linear relationship. This limited impact may be a result of the inability of multi-Gaussian  $K$ -fields, and the related spatial structures within the aquifer, to influence the observed hydraulic response (Zinn and Harvey, 2003). The level of connectivity within the  $K$ -field has been shown to strongly influence the transport behaviour (Zinn and Harvey, 2003) and hydraulic response to pumping (Lee et al., 2007). More advanced stochastic modelling approaches (such as multiple-point geostatistical simulations (Mariethoz et al., 2010)) may be needed to further investigate the impacts of spatial structures within the aquifer. Nevertheless, this study represents a first step to understanding the impact of aquifer heterogeneity upon the representative stream discharge length.

Previously work has shown that groundwater flow (in a 2-dimensional isotropic multi-Gaussian  $K$  field) through a given number of correlation length approaches the flow rate governed by the geometric mean hydraulic conductivity of the aquifer (Gomez-Hernandez and Gorelick, 1989; Dagan, 1997; Zinn and Harvey, 2003). This study has shown that the variability in groundwater discharge ( $CV(Q_{eff}^{x,y})$ ) starts to decrease and approach the mean groundwater discharge after 2.5 correlation length. Due to the design of the model domain, this was only achieved for  $\tau = 10$  m and 50 m. Assuming stationarity and that this estimate of groundwater discharge is accurate, the estimated discharge rate can be

up-scaled to the entire stream length with those aquifer characteristics (Bear, 1972). In practice, locating a well at a distance of 2.5 correlation length from the stream will be problematic given that the correlation length within the aquifer is rarely known and likely to be scale-dependent.

The influence of vertical heterogeneity in hydraulic conductivity was not considered in this study. The Hall and Moench (1972) solution used in the theoretical modeling assumes constant transmissivity and neglects vertical flow. Those piezometers in close proximity to the stream will be influenced by both vertical and horizontal flow paths which are not accounted for in this model setup. This will introduce errors into the estimation of the hydraulic properties for those piezometers (see Sophocleous et al. (1991)). For the field example, we have assumed a constant storage coefficient. The accuracy of the field groundwater discharge estimates may be improved in future by combining stream stage change experiments with aquifer pumping tests; this would provide estimates of both Keff and aquifer storage coefficients (Rötting et al., 2006).

## 2.6 Conclusions

The use of Darcy's law to obtain groundwater discharge estimates to streams is widely accepted. This investigation has shown that the capacity to up-scale point discharge estimates to capture the regional scale of discharge to a stream is limited. Using a theoretical investigation it was demonstrated that the representative stream length is approximately equal to the distance of a piezometer from a stream. The correlation length does not affect the representative stream length. The theoretical investigation was complemented by a field application, the results of which showed a clear reduction in the variability in effective hydraulic conductivity and groundwater discharge as the distance between the stream and piezometer increases.

## Acknowledgments

Funding for this research was provided by the National Centre for Groundwater Research and Training, an Australian Government Initiative, supported by the Australian

Research Council and the National Water Commission, and the Goyder Institute for Water Research of South Australia. The authors would like to acknowledge Mark de Jong and the staff of the Millicent, Department of Environment, and Water and Natural Resources office for access to data and field assistance. Also thanks to Cameron Wood, Nikki Harrington, Chani Welch, Nick White, Luke Peeters, Lawrence Burk, and Jordi Batlle-Aguilar for assistance in the field. The authors wish to thank Geoff Syme and two anonymous reviewers for comments that strengthened this work.

## Chapter 3

# Estimating seepage flux from ephemeral stream channels using surface and ground-water level data

Noorduijn, S.L., Shanafield, M., Trigg, M. A., Harrington, G. A., Cook, P. G., and Peeters, L. (in press) Estimating seepage flux from ephemeral stream channels using surface and ground-water level data, *Water Resour. Res.*, 50, doi:10.1002/2012WR13424



### 3.1 Abstract

Seepage flux from ephemeral streams can be an important component of the water balance in arid and semi-arid regions. An emerging technique for quantifying this flux involves the measurement and simulation of a flood wave as it moves along an initially dry channel. This study investigates the usefulness of including surface water and groundwater data to improve model calibration when using this technique. We trialed this approach using a controlled flow event along a 1387 m reach of artificial stream channel. Observations were then simulated using a numerical model that combines the diffusion wave approximation of the Saint-Venant equations for streamflow routing, with Philip's infiltration equation and the groundwater flow equation. Model estimates of seepage flux for the upstream segments of the study reach, where streambed hydraulic conductivities were approximately  $101 \text{ m d}^{-1}$ , were on the order of  $10^{-4} \text{ m}^3 \text{ d}^{-1} \text{ m}^{-2}$ . In the downstream segments, streambed hydraulic conductivities were generally much lower but highly variable ( $\sim 10^{-3} - 10^{-7} \text{ m d}^{-1}$ ). A Latin Hypercube Monte Carlo sensitivity analysis showed that the flood front timing, surface water stage, groundwater heads and the predicted stream flow seepage were most influenced by specific yield. Furthermore, inclusion of groundwater data resulted in a higher estimate of total seepage estimates than if the flood front timing were used alone.

### 3.2 Introduction

Groundwater recharge from ephemeral and intermittent systems plays an important role in sustaining water resources in arid and semiarid environments (Sophocleous, 2002). Quantifying the contribution from ephemeral streams to the water balance is important in such environments, where surface water resources are limited and in great demand (Winter et al., 1998). In particular, this requires knowledge of the spatial variability of recharge along the ephemeral stream channels that can be used to inform management strategies for the capture and storage of the water resource (Callegary et al., 2007). However, the limited predictability of stream flow events in arid and semiarid environments hinders the application of traditional field-based techniques to estimate seepage and re-

charge.

Direct and indirect methods have been developed that assess recharge in arid environments at the point/local and regional scales (Goodrich et al., 2004); these methods include the use of geochemical tracers (Harrington et al., 2002; Vanderzalm et al., 2011), analytical and numerical modeling of groundwater mounding (Abdulrazzak, 1983; Walters, 1990; Mudd, 2006; Chenini and Ben Mammou, 2010), reach-scale water balances (Keppel and Renard, 1962; Knighton and Nanson, 1994; Ruehl et al., 2006), surface geophysics (Pool and Eychaner, 1995; Callegary et al., 2007), and water, solute, and heat transport modeling in the unsaturated zone (Conant Jr, 2004; Su et al., 2004; Dahan et al., 2007, 2008; Kalbus et al., 2008; Dahan et al., 2009; Shanafield et al., 2010). The accuracy of up-scaling point and down-scaling regional seepage estimates has also proven challenging (Cushman, 1986; Wood, 2009).

Advancements in remote monitoring technology have led to the development of techniques involving the use of ephemeral river flood event data to quantify surface water infiltration, and hence groundwater recharge (Niswonger et al., 2008). Previously, this concept had been applied in agricultural fields at the furrow scale to determine infiltration rates (Scaloppi et al., 1995; Camacho et al., 1997); only recently has it been applied to larger natural and artificial channels to aid with catchment water management (Niswonger et al., 2008). Mudd (2006) demonstrated theoretically that infiltration has an appreciable impact on the flood front movement, i.e., slowing flood front movement where infiltration is high. This approach has been further developed to incorporate variably saturated flow. Furthermore it has been modified for both the kinematic and diffusion wave approximation of the Saint-Venant equations for the flood wave routing (Niswonger and Prudic, 2004; Niswonger et al., 2005; Shanafield et al., 2012).

Niswonger and Prudic (2005) and Niswonger et al. (2008) developed a method that combined the kinematic wave approximation of the Saint-Venant equations and Philip's infiltration equation, and was linked to the groundwater flow equation. This provided a framework enabling the use of streamflow-front velocity to determine streambed hydraulic conductivity for an initially dry channel. This package was developed from the streamflow routing package (SFR2) for MODFLOW-2000 for the simulation of gravity

induced unsaturated flow beneath streams (Niswonger and Prudic, 2004). The kinematic wave approximation is the simplest approximation of the Saint-Venant equations and assumes that the water surface is equal to the bed slope i.e., the pressure force, local and convection acceleration force terms are negligible. This method proved successful in steeper downhill sloped ephemeral streams with fast flow (Niswonger et al., 2005).

The kinematic wave approximation can be an inappropriate simplification where the channel slope is shallow and where bed slope can be locally negative (Maidment, 1992). In these instances including the pressure force term, as a minimum (i.e., diffusion wave approximation or full Saint-Venant equations), is necessary to account for the shallow or negative slopes and the resultant backwater effects on upstream flows and /or surface water levels. The more complicated full Saint-Venant equations can prove unsuitable due to numerical instabilities and have a high computational demand; therefore the diffusion wave approximation proves to be the most suitable model (Chow et al., 1988).

For this study the diffusion wave approximation of the Saint-Venant equations provided the most appropriate solution due to its ability to cope with shallow bed slope and negative gradients (Maidment, 1992). Similarly the predicted average kinematic wave number for the study reach was below the accepted value for the use of the kinematic wave model (Woolhiser, 1974). The maximum Froude number for the reach was 0.07, also indicating that the most appropriate Saint-Venant approximation is the diffusion wave (Vieira, 1983).

Several models for diffusion wave routing have already been developed. DAFLOW (Jobson and Harbaugh, 1999) and MODFLOW-SWR1 (Hughes et al., 2012), are diffusion wave models, however they do not simulate unsaturated water movement. As a result they are best suited to connected systems where surface water – groundwater interactions are governed by Darcy's law. Similar to the Niswonger et al. (2008) kinematic model, Shanafield et al. (2012) linked a diffusion wave routing of surface flow with the Philip's equation for infiltration and MODFLOW for groundwater response. This model was therefore chosen for this study because it allowed for the advancement of a flood front along an initially dry, mild sloped channel and the resultant aquifer response to be used to calibrate for changes in hydraulic conductivity along the study reach.

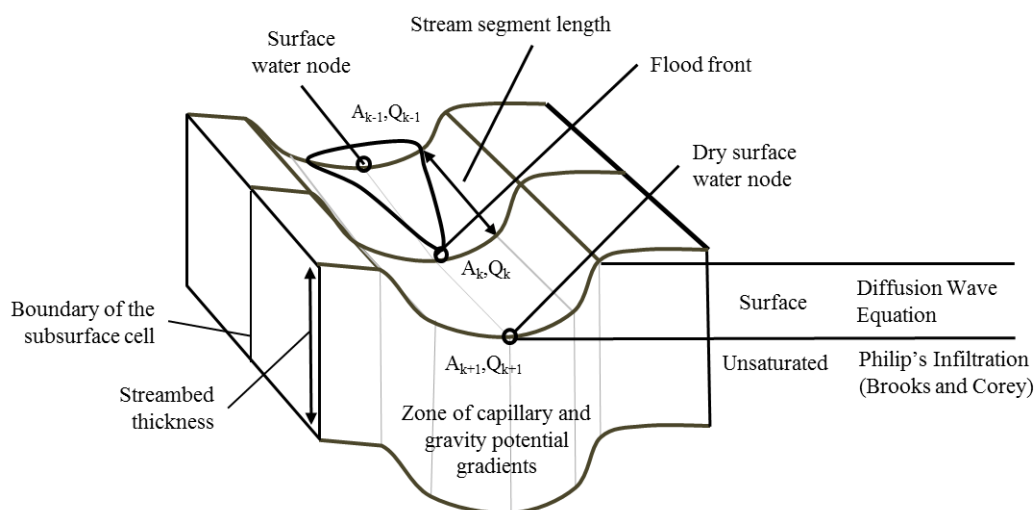


Figure 3.1: Conceptual diagram of the diffusion wave - MODFLOW model (based on Niswonger et al. (2008)) showing the surface and subsurface discretization for flow calculation, where  $A$  is channel area ( $L^2$ ) and  $Q$  is flow ( $L^3T^{-1}$ ).

The aim of this study was to investigate how the inclusion of surface water and groundwater head data in the calibration of a coupled surface-water-flow – infiltration – groundwater flow model aids the estimation of seepage flux. This was achieved using a controlled flow event in an artificial channel, and a recently developed model that couples the diffusion wave approximation to Philip's infiltration and MODFLOW (Shanafield et al., 2012). Previous applications of the model have not considered stream stage or groundwater head data in the calibration processes, which we show is valuable. We assess the sensitivity of the flood front flow, surface water stage and groundwater head objective functions as well as the estimated total seepage to various input parameters using a Latin Hypercube Monte Carlo sensitivity analysis (Saltelli et al., 2008).

## 3.3 Background

### 3.3.1 Theory

The diffusion-wave approximation combines the continuity and momentum equations, assuming that acceleration forces can be neglected (Moussa and Bocquillon, 1996). Following Maidment (1992), the continuity equation can be expressed as;

$$\frac{\partial Q}{\partial x} + \frac{\partial A}{\partial t} = 0 \quad (3.1)$$

and the momentum equation can be expressed as;

$$g \left( \frac{\partial h_s(t)}{\partial x(t)} \right) - g (S_o - S_f) = 0 \quad (3.2)$$

where  $Q$  is flow ( $L^3T^{-1}$ ),  $A$  is the cross-sectional area of the channel ( $L^2$ ),  $h_s$  is the water surface elevation in the channel ( $L$ ),  $x$  is the length in the direction of flow ( $L$ ),  $S_o$  is the channel slope ( $LL^{-1}$ ),  $S_f$  is the friction slope ( $LL^{-1}$ ), and  $t$  is time ( $T$ ).

The combination of these equation yields the one-dimensional diffusion wave approximation given as (Panday and Huyakorn, 2004);

$$\frac{\partial}{\partial x} \left( k_x \left( \frac{\partial h_s}{\partial x} \right) \right) - \frac{\partial (Bh_s)}{\partial t} - Aq_g = 0 \quad (3.3)$$

where  $B$  is the cross-sectional top width ( $L$ ),  $k_x$  is the channel conductance term ( $L^3 T^{-1}$ ), and  $q_g$  is the flux per unit volume seepage to the subsurface ( $T^{-1}$ ). This equation has the same form as the groundwater flow equation (Panday and Huyakorn, 2004), making it possible to solve using sparse-matrix solvers identical to those in MODFLOW (Harbaugh, 2005). The proportion of infiltration occurring during the initial wetting up of the streambed profile has been shown to be significant when compared to the total seepage loss (Batlle-Aguilar and Cook, 2012; Blasch et al., 2013). This is not considered when a constant infiltration rate is applied uniformly along the channel in question and can result in errors in total seepage loss estimates (Walters, 1990; Hameed et al., 1996; Morin et al., 2009). Philip's infiltration equation (Philip, 1957, 1958) was used to incorporate the transient infiltration rate during the onset of flow, driven by the large capillary gradient at the flood front. The assumptions of this approach include one-dimensional, vertical, homogeneous flow and can be written as:

$$I = \frac{1}{2} S t_w^{-0.5} + K_s \quad (3.4)$$

where  $I$  is infiltration ( $L T^{-1}$ ),  $t_w$  is the time since initial channel wetting by flow ( $T$ ),  $K_s$  is the saturated hydraulic conductivity of channel sediments ( $L T^{-1}$ ), and  $S$  is sorptivity ( $L T^{-1/2}$ ), which is a function of the stream depth, sediment water retention curve, relative hydraulic conductivity, and the initial and saturated water content of the streambed,

$\theta_i$  and  $\theta_s$ . Following Philip (1958), the effects of stream depth on sorptivity are also incorporated, and sorptivity is expressed as:

$$S^2 = 2K_s (\theta_s - \theta_i) \left[ \int_{\psi_i}^0 K_r(\psi) d\psi + h_s \right] \quad (3.5)$$

where  $\psi$  is the capillary pressure potential (L) and  $K_r(\psi)$  is the relative hydraulic conductivity as a function of capillary pressure potential (dimensionless). Philip's infiltration equation was coupled to the Brooks and Corey (1964) soil-water characterization curve to estimate the changes in saturation and capillary gradient as the flow moved down gradient. This analytical solution assumes that both the hydraulic conductivity and soil water diffusivity are a function of sediment water content (rather than depth). Therefore these assumptions are only valid where there is no significant vertical heterogeneity in the streambed sediments.

When the groundwater table is lower than the streambed, infiltration to the groundwater is incorporated into the seepage term as:

$$Aq_g = PI \quad (3.6)$$

where  $P$  is the channel wetted perimeter (L) and  $I$  is the infiltration rate ( $LT^{-1}$ ). When the water table rises to the base of the streambed and above, the seepage to the groundwater is calculated as:

$$Aq_g = K_s Pl \frac{(h_g - h_s)}{b} \quad (3.7)$$

where  $K_s$  ( $LT^{-1}$ ) is the hydraulic conductivity of channel sediments,  $h_g$  (L) is the groundwater head in the underlying cell,  $l$  is the length of the reach (L), and  $b$  is the average streambed thickness (L). Combining the surface and subsurface flow equations enables estimation of the groundwater response to a surface flood event (Keppel and Renard, 1962). To simulate the connection between surface water and groundwater flow, the diffusion-wave approximation and Philip's infiltration equations are combined and coupled with the groundwater flow equation (Panday and Huyakorn, 2004). The surface water level and groundwater heads are combined into one matrix and determined simultaneously using a Newton-Krylov solver in the NWT package (Niswonger et al., 2011).

The model developed by Shanafield et al. (2012) couples the one-dimensional diffusion-wave approximation with Philip's infiltration equation (Philip, 1957, 1958) and MODFLOW-NWT (Niswonger et al., 2011) providing a useful tool for the simulation of within channel flow events and associated groundwater response (Figure 3.1).

### 3.3.2 Field Site

This study was performed on the Western Reflows Floodway (WRF), a newly graded, un-lined artificial water conveyance channel located in the South East of South Australia (lat.  $37^{\circ}13'16$  long.  $140^{\circ}29'21$ ) (Figure 3.2). The channel was designed to convey water northward to the RAMSAR listed Coorong wetlands to help maintain ecological water requirements (Harding, 2007). Construction of the trapezoidal channel was completed in 2010, and remained unused until a controlled flow event in May 2011.

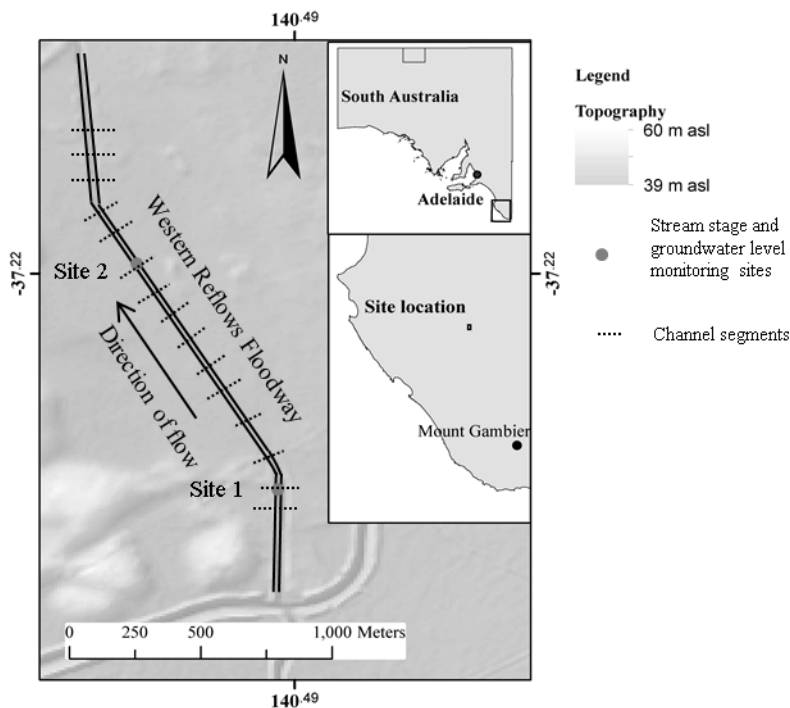


Figure 3.2: Map of the Western Reflows Floodway (WRF) study reach in the South East region of South Australia. Dashed lines define segment boundaries for the model (surface water node, see Figure 3.1) and identify the location of surface water level monitoring. Topography is shown as metres above sea level

The study focused on a 1387 m reach of the WRF north of the Callendale Flow Regulator (CFR) on Drain M (lat.  $37^{\circ}13'41.26$  long.  $140^{\circ}29'27.57$ ). The reach is located

within a seven-year-old blue gum (*Eucalyptus globulus*) plantation, however the channel itself is bare in the upstream section and sparsely vegetated with grass and reeds in the downstream section. At the field site, the Semaphore Sand member, an unconsolidated white bioclastic quartz-carbonate sand of modern beaches and transgressive dune fields extends from the surface to approximately 5 m depth (Fariclough, 2010). During construction, a clay layer was observed beneath the channel; the depth to this layer decreases downstream from 0.5m to 2.0 m below the base of the channel. The WRF was designed to convey flows of less than  $3 \text{ m}^3 \text{ s}^{-1}$ , and has a uniform base width of 20 m with  $45^\circ$  banks. The average slope of the study reach is  $0.0002 \text{ (m m}^{-1}\text{)}$ . The direction of regional groundwater flow is towards the northeast and depth to groundwater in the area is approximately 4 m below ground level (bgl). However, beneath the channel the depth to groundwater is less (0.5-2 m bgl) suggestive of water table mounding due to increased recharge along the bare channel relative to the adjacent forest plantation.

## 3.4 Methodology

### 3.4.1 Field Methods

A controlled flow event was performed at the site from 19 May - 2 June 2011 by closing the CFR on Drain M and allowing water to flow into the WRF. The study reach was divided into 15 segments; flood front (*ff*) timing and surface water level (i.e., stage) were monitored at each segment boundary. Prior to the event, two additional monitoring sites, located approximately 500 m apart, were instrumented to measure shallow groundwater head and surface water level. At these sites (Site 1 and 2; Figure 3.2) groundwater head was measured in drive-point piezometers installed at 1.5 m below ground level in the center of the channel, assumed to be the depth of the streambed. All surface water levels were monitored at the channel thalweg. Pressure transducers (In-Situ Inc LevelTROLL® 300 Series,  $\pm 0.2\%$  accuracy, and In-Situ Inc. BaroTROLL®,  $\pm 0.05\%$  accuracy) were used to record stream depth and groundwater heads at one-minute intervals. Only the data for the period when flow commenced at the upstream boundary until flow reached the downstream boundary is of relevance to the model calibration.

Table 3.1: Description of model parameters. Where appropriate the estimated measurement error for each parameter has been identified based on the authors judgement.

Type	Parameter	Units	Error (%)
Fixed for each segment			
	$s_l$ Segment length	m	5
	$s_t$ Segment thalweg	m asl	10
	$S_o$ Segment slope <sup>§</sup>	-	10
	$B_s$ Streambed thickness <sup>§</sup>	m	50
	$\theta_s$ Streambed saturated water content <sup>§</sup>	-	10
	$\theta_i$ Streambed initial water content <sup>§</sup>	-	10
	$\theta_r$ Streambed residual water content <sup>§</sup>	-	100
	$\eta$ Brooks-Corey coefficient <sup>§</sup>	-	50
	$P$ Channel wetted perimeter	m	10
	$r$ Channel hydraulic radius	m	10
	$w$ Channel width	m	10
For entire model			
	$Q_i$ Inflow rate <sup>§</sup>	$\text{m}^3\text{s}^{-1}$	50
	$B_a$ Aquifer thickness <sup>§</sup>	m	75
	$S_y$ Specific yield <sup>§</sup>	-	25
	$h_g^i$ Initial groundwater head <sup>§</sup>	m	5
Estimated			
	$K_s$ Streambed hydraulic conductivity <sup>§</sup>	$\text{m s}^{-1}$	-
	$K_a$ Aquifer hydraulic conductivity	$\text{m s}^{-1}$	-
	$n$ Manning's $n$ roughness coefficient <sup>§</sup>	$\text{s m}^{-1/3}$	15
Calculated			
	$ff$ Flood front arrival for each segment	h	2
	$h_s$ Surface water level for site 1 and 2	m	5
	$h_g$ Groundwater head for site 1 and 2	m	5

<sup>§</sup>Parameters included in the Monte Carlo analysis.  $K_s$  was included per segment.

Flow into the study reach was determined by manual flow gauging at the upstream boundary of segment 1. A Marsh-McBirney Flo-Mate was used to estimate flows following the area-velocity method (Hipólito and Loureiro, 1988). Due to the transience of the flow as the flood wave passed, the flow gauging began with one measurement of flow in the channel and increased to 12 lateral measurements as the rate of change in surface water level decreased. This constrained error and minimized the time interval between gaugings. The time between subsequent gaugings was between two and 12 minutes depending on the number of velocity measurements. The flood front progression down the channel was tracked using handheld Garmin GPS units.

Streambed sediment properties for the study reach were determined from samples

collected at Sites 1 and 2. Site 1 was sand, which appeared to extend downstream to segment 4. At Site 2 the streambed sediments had greater clay content, which remained present in segments 5 to 11. Sediment samples from the top 0.4 m of the streambed were collected and analyzed using the filter paper method (Fawcett and Collis-George, 1967; Greacen et al., 1989) and hanging water column to estimate the water retention curves and the Brooks and Corey coefficient (Brooks and Corey, 1964). The channel sediment moisture profile was assumed to be initially at equilibrium; for example, where the perched water table was at 1.5 m, the surface matric potential was assumed to be -1.5 m. The initial  $\theta_i$  was then derived from the water retention curve. The residual ( $\theta_r$ ), and saturated ( $\theta_s$ ) sediment water content was also estimated using the water retention curves (see Table 3.1). No evaporative losses were considered due to the short duration of flow (2.28 h travel time) within the channel.

### 3.4.2 Modeling

The field data provided a framework to construct a numerical model of the captured flow event. The objective of the model calibration was to quantify the spatial variability of the streambed hydraulic conductivity ( $K_s$ ) and thus seepage flux. The sensitivity of the calibrated model to each of the input parameters was investigated, as was the uncertainty in total seepage flux for the reach (see section 3.2.2).

The 15 channel segments provided the surface discretization for the model. A site survey determined the channel cross-section geometry at the upstream and downstream end of each segment (Table 3.2). Channel surface water hydraulic properties (wetted perimeter, channel width, and hydraulic radius) for each segment were calculated for ten stream stage depth (0.01 m - 0.7 m). Finer discretization of the hydraulic properties at shallow stream stage depth was necessary to account for vertical variations in friction, which was particularly important in this study as flow depth varied from zero to full event depth (0.5 m) and resistance values are strongly depth, and hence flow dependent (Morvan et al., 2008). The Manning's  $n$  roughness coefficient was estimated by using an equivalent roughness parameter ' $k$ ' described in USACE (1991) and Brunner (2010). An appropriate  $k$  value was determined by setting  $n$  as 0.024 at a surface water depth of 0.5 m, which is

Table 3.2: Parameters values for the 15 segments within the WRF study reach that were fixed during the calibration process. These values were allowed to vary during the sensitivity analysis. Refer to Table 3.1 for parameter definitions and estimated measurement error.

#	Segment Parameters		Streamflow Parameters		Seepage Parameters			Groundwater Parameters			
	$s_l$	$s_l$ , m asl	$S_o$	$w_b$ , m	$w_a$ , m	$\theta_s$	$\theta_l$	$\theta_r$	$\eta$	$S_y$	$h_g^l$ , m asl
1	121	40.48	0.00017	19.29	23.85	0.22	0.17	0.04	8	0.180	39.053
2	52	40.433	0.00090	19.15	24.79	0.22	0.17	0.04	8	0.180	39.283
3	77	40.473	-0.00052	18.91	25.19	0.22	0.17	0.04	8	0.087	39.283
4	86	40.441	0.00037	17.08	22.76	0.22	0.36	0.08	2.5	0.064	39.540
5	89	40.449	-0.00009	17.88	22.10	0.36	0.36	0.08	2.5	0.032	39.671
6	93	40.422	0.0029	15.83	22.39	0.36	0.17	0.08	2.5	0.032	39.784
7	93	40.388	0.0037	14.89	22.22	0.36	0.36	0.08	2.5	0.170	39.899
8	80	40.402	-0.0018	19.20	20.16	0.36	0.36	0.08	2.5	0.018	39.899
9	82	40.423	-0.00026	17.70	22.14	0.36	0.17	0.08	2.5	0.020	39.899
10	108	40.268	0.00144	21.00	23.72	0.36	0.36	0.08	2.5	0.020	40.070
11	92	40.249	0.00021	16.90	21.66	0.36	0.36	0.08	2.5	0.034	39.590
12	94	40.301	-0.00055	17.70	21.97	0.36	0.25	0.08	2.5	0.071	39.347
13	94	40.247	0.0057	17.70	21.64	0.36	0.25	0.08	2.5	0.098	39.099
14	96	40.195	0.0054	19.32	22.59	0.36	0.36	0.08	2.5	0.091	39.099
15	130	40.235	-0.00031	1810	22.05	0.36	0.30	0.08	2.5	0.133	38.820

$w_b$ , m width at base of the channel  
 $w_a$ , m width of channel at 0.5 m water depth

within the range expected for an excavated earthen channel (0.018-0.025; Chow, 1959). All  $n$  values decreased from 0.1 at a depth of 0.01 m, to 0.024 at 0.5 m depth. The upper Manning's  $n$  roughness coefficient was selected as a reasonable estimate of the channel roughness at shallow depth.

The downstream boundary condition is a critical depth condition at which the Froude number is equal to one. To ensure this boundary did not influence the surface water solution, the length of the last segment in the model was increased by 100 m to prevent the flood front reaching the downstream boundary within the calibration period. Time step length was assigned according to the time for the flood front to progress from one segment boundary to the next and ranged from 270 – 961 seconds. The timing of full channel width flow was also used in the calibration for comparison. In this study, the small difference between the flood front and full channel width flow coupled with the observed shape of the front suggested that flood front timing was an appropriate measure of the flood front velocity.

Initial groundwater head ( $h_g^i$ ) below the channel, obtained from groundwater monitoring Sites 1 (segment 2) and 2 (segment 10), were 1.41 m and 0.37 m respectively. Additional groundwater head data from a drive-point located at the downstream end of the channel was used as the groundwater head for the last segment. The groundwater head for each segment was interpolated between the measured groundwater heads from these three sites. Only locations where both surface water levels and groundwater head data were collected were used in the model calibration. Specific yield ( $S_y$ ) was estimated from the water retention curve and the initial.  $S_y$  was then estimated as the difference between the total porosity (equal to  $\theta_s$ ) and the initial surface soil moisture.

Discretization in the direction of flow was approximately 100 m, equal to the segment length (Table 3.2). The groundwater model boundary conditions were set a sufficient distance away (4 km) from the channel, to limit their influence on the solution. The cells beneath and directly adjacent to the channel had a cell width ( $y$ -direction, perpendicular to channel) of 25 m. The cell width increased to 500 m at a perpendicular distance of 100 m from the channel edge. Cell depth was set to 2.5 m. Aquifer hydraulic conductivity ( $K_a$ ) was assumed to be equal to streambed hydraulic conductivity ( $K_s$ ).

### 3.4.2.1 Model Calibration

Model calibration was undertaken using the parameter estimation program PEST (Doherty, 2010) which uses a least squares fitting routine and a Gauss Marquardt Levenberg method to minimize a user-defined objective function;

$$\phi_k = \sum_{k=1}^{N_{obs}} (w_k x_k^m - w_k x_k^s)^2 \quad (3.8)$$

where  $\phi_k$  is the objective function value (units dependent on  $x$ ),  $w_k$  is the weight applied to the difference between the measured ( $x_m^k$ ) and simulated ( $x_s^k$ ) parameter of the same type  $k$ , and  $N_{obs}$  is the total number of measured parameter values of the same type. The objective function is calculated for each data type. During the optimization process, PEST solves global objective function which incorporates the different types of data. We impose a weighting on each data type by the following equation:

$$w_k = \frac{1}{\sigma \sqrt{N_{obs}}} \quad (3.9)$$

where  $\sigma$  was the standard deviation in observation data of the same type, this normalized the weightings according to the different data type measurement values and number of measurements (McCallum et al., 2012). Model parameters are defined in Table 3.2.

Three different scenarios were used to investigate the impact of including different data types (namely flood front timing, surface water level and groundwater head) on model calibration. In the first scenario only flood front timing data was used in the objective function, whereas in the second and third scenarios all three data types were used (Table 3.3). In all three cases, streambed saturated hydraulic conductivity ( $K_s$ ) was the parameter to be estimated, plus in the third scenario, Manning's roughness coefficients ( $n$ ) were also estimated parameters.

A simulated flow of  $0.05 \text{ m}^3\text{s}^{-1}$  into each segment was the criteria used to identify the flood front arrival time at each segment boundary; the streambed was considered dry for flow values below  $0.05 \text{ m}^3\text{s}^{-1}$ . This represents the flow at a stage depth of 0.01 m as determined from the manual gauging at segment 1.

The models were run for a period of 22 h in order to simulate the observed surface

water level data and groundwater head data up to a time when the flow had stabilized. The recession of flow was not included due to lack of inflow data; this would prove interesting for future studies.

### 3.4.2.2 Sensitivity Analysis

A Monte Carlo analysis was performed to investigate the sensitivity of the total seepage flux, estimated using the calibrated model, to the input parameters. Latin-hypercube sampling (LHS) was used to generate the multivariate parameter distributions used for the Monte Carlo simulations. LHS is a form of stratified random sampling that reduces the number of simulations necessary for the Monte Carlo analysis. Twenty-seven parameters were considered in the Monte Carlo simulations (Table 3.1) and a sample size of  $N = 10,000$  was chosen (Iman and Helton, 1988). Values for the 27 input parameters were selected from a normal distribution with standard deviation equal to the standard measurement error (see Table 3.1). Measurement errors were based on the authors judgement. Streambed saturated hydraulic conductivities ( $K_s$ ) were assumed to be log-normally distributed for the purpose of the Monte Carlo analysis. A reasonable error was used for the  $K_s$  based on observed sediment types within the channel. Model runs that did not converge within 10 times the average run time were observed to produce unrealistic output data and were discarded. The calibrated model from scenario D2 was used as the base case in the sensitivity analysis.

The model output was assessed in terms of different objective functions: flood front flow ( $ff$  flow)  $\phi$ , surface water level  $\phi$ , groundwater head  $\phi$ . Total simulated seepage along the channel was also compared, defined as the sum of the seepage flux from each of the segments over the total simulation period (i.e., 22 h). The  $ff$  flow  $\phi$  represents the deviation of the flow output from the observed flow at each segment boundary i.e., flood front arrival indicated by a flow of  $0.05 \text{ m}^3\text{s}^{-1}$ .

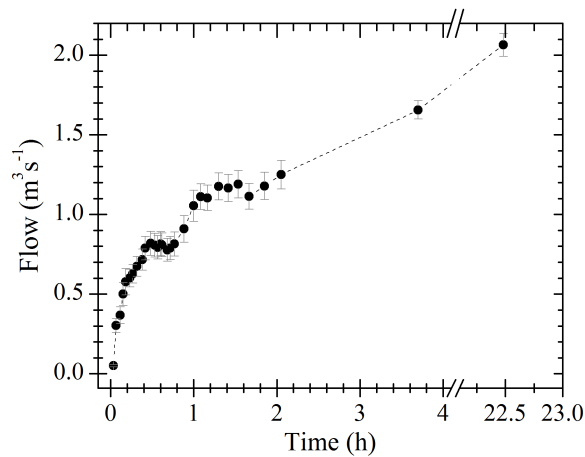


Figure 3.3: Inflow flood hydrograph determined by manual gauging at the upstream boundary of the WRF reach. The area-velocity technique was applied to determine flow. Error bars are calculated from a 5% measurement error with an additional error calculated from the change in flow during the period of each flow measurement. The total estimated error ranged from 15% at the beginning of the event to 5% for the steady state.

## 3.5 Results

### 3.5.1 Experimental Results

Flow into the study reach commenced at 12:28 pm on 19 May 2011. The maximum flow into the reach was  $2.6 \text{ m}^3\text{s}^{-1}$ , occurring 25 h after the onset of flow (Figure 3.3). A distinctive step pattern was observed in the rising limb of the flow, which was also present in the surface water level at the upstream boundary, most likely indicating the flow is utilizing storage in the system upstream of the study reach at this point. Total time for the flood front to travel the 1387 m to the end of the study reach was 2.28 h (flow initiation) and 2.31 h (full channel inundation) Figure 3.4). For the majority of segments, full channel flow occurs within minutes of the initial flood front passing. However, there is a greater delay for segments 3-7 on the order of 9 minutes. This increased lag can be attributed to the presence of ponded surface water within the channel resulting in an acceleration of the flood front (i.e., piston flow within the ponded water).

The maximum surface water level of 0.5 m at the upstream boundary was reached 14.2 h after the onset of flow. The highest stage observed along the reach occurred at the same time in segment 10 (0.6 m). The streambed thalweg greatly influenced the shape of the wave, as seen in the large positive (downstream) streambed gradient at segment 10

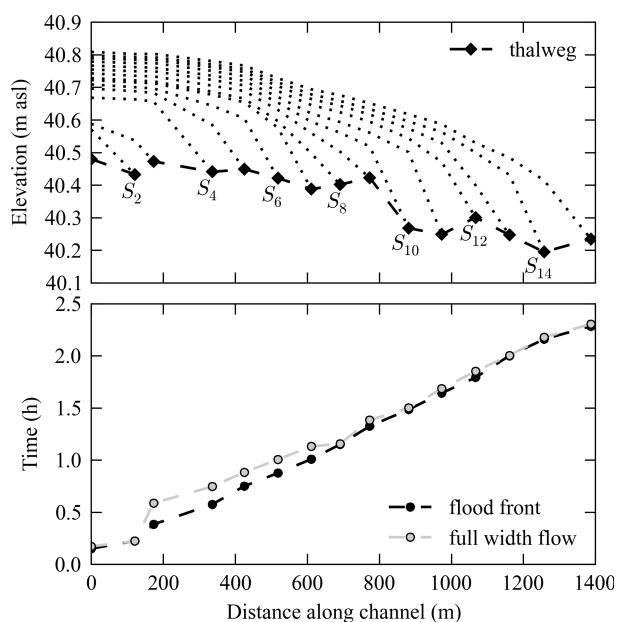


Figure 3.4: Timing and shape of the flood-wave at each segment boundary (grey diamond and labeled  $S_2$ ,  $S_4$ , etc) determined from pressure transducer data and site survey at each boundary. The circles and dashed line (unfilled) show the cumulative travel time of the flood front for both the initial flow (filled circles) and flow at full width inundation (open circles).

and the negative (upstream) streambed gradients in the previous segments (Figure 3.4).

The gradient in the surface water clearly decreased for segments 8 and 9.

The average, minimum, and maximum flood front velocities were  $0.17 \text{ m s}^{-1}$ ,  $0.12 \text{ m s}^{-1}$  (segment 4), and  $0.29 \text{ m s}^{-1}$  for (segment 15), respectively. The lower flood front velocities were associated with negative bed slope, especially in segments 3 and 9.

### 3.5.2 Model Results

Table 3.3: Outline of the calibration scenarios tested, where streambed hydraulic conductivity is  $K_s$ , surface water level is  $h_s$ , and groundwater head is  $h_g$ . Manning's  $n$  was allowed to vary for 10 surface water stages (sws) for Scenario 3.

Scenario	Estimated Parameters	No. Segments	Objective function
D1	$K_s$	15	flood front timing
D2	$K_s$	15	flood front timing, $h_s$ , $h_g$
D3	$K_s$ Manning's $n$	15	flood front timing, $h_s$ , $h_g$

Of the three scenarios used to calibrate the model (D1-D3, Table 3.3) scenario D2

provided a marginally better fit to the observed surface water level and groundwater head data (Figure 3.5). The error in flood front timing for scenario D2 was only slightly higher than for scenario D1 where flood front timing was the only data type used in the objective function. Comparing the results of scenario D3 with those of scenario D2 suggests the treatment of Manning's  $n$  as an estimated parameter in the model optimization did not improve the calibration for flood front timing, and actually worsened the calibration for surface water level and groundwater head. The spatial variability in estimated seep-

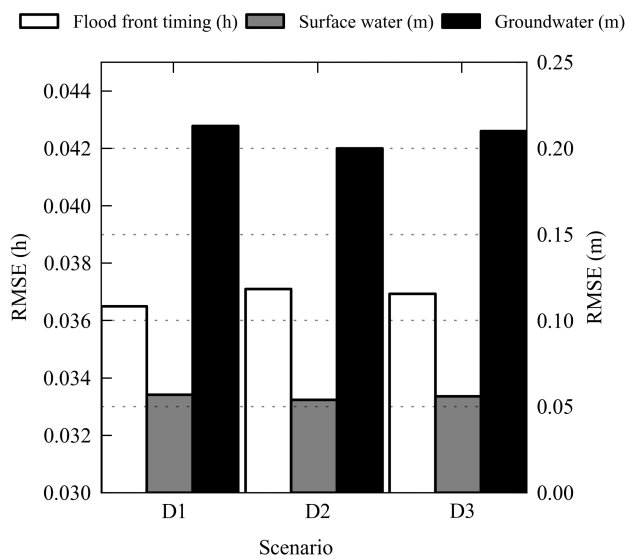


Figure 3.5: The root mean squared error (RMSE) associated with different data types for three different calibration scenarios (see Table 3.3).

age flux along the channel for the three scenarios displays similar trends (Figure 3.6). The scenarios exhibits a general trend from relatively high values in the upper segments ( $10^{-4}$  to  $10^{-3}$   $\text{m}^3\text{d}^{-1}\text{m}^{-2}$ ) to much lower values in the lower segments ( $10^{-7}$  to  $10^{-4}$   $\text{m}^3\text{d}^{-1}\text{m}^{-2}$ ), although these fluxes are extremely variable from one segment to the next. Variation in estimated seepage flux between the three scenarios is more pronounced in the downstream segments, in particular those with a lower seepage flux estimate. The low seepage fluxes observed in the downstream segment may be attributed to the clay layer observed beneath the channel. This clearly demonstrates the value of including both surface water level data and groundwater head data as calibration constraints when modeling seepage flux.

The simulated surface water and groundwater response for Site 1 is consistent with

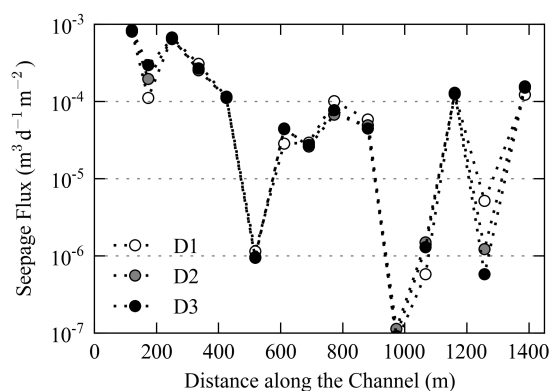


Figure 3.6: Estimated seepage flux (solid circles) along the channel for each model calibration scenario.

the measured data (Figure 3.7). During the initial 4 h of the simulation the groundwater response is overestimated by 0.2 m, subsequent to this the simulated groundwater head fits well to the observed response. At Site 2 accumulated errors in the timing of the flood front arrival resulted in pre-emptive increase in the both the surface water and groundwater response (Figure 3.7) e.g., the simulated rise in groundwater head occurred 19 minutes before the observed response. In the long term (post 4 h) the surface water response was consistently underestimated by up to 0.06 m; this response is not observed in the simulated groundwater head.

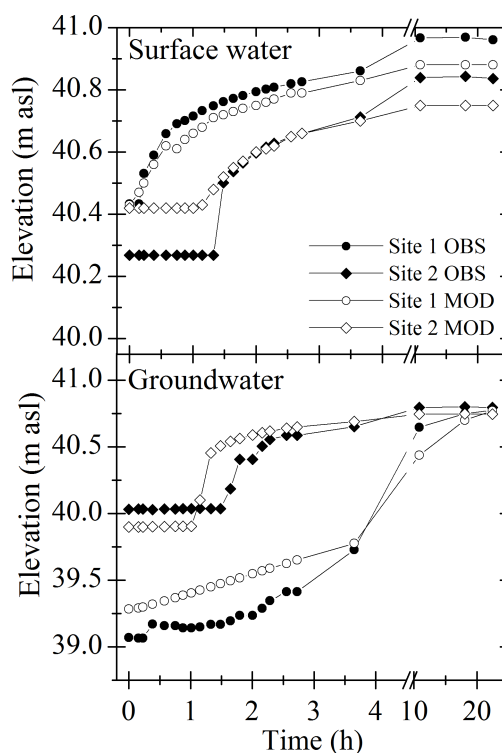


Figure 3.7: Observed (OBS) and modeled (MOD) surface water levels and groundwater heads at Sites 1 and 2 (see Figure 3.2 for locations).

Towards the end of the simulation, when conditions are assumed to be near steady state, the simulated surface water level was below the measured value by 0.08 m for Site 1 and 0.13 m for Site 2. For both sites, the surface water level remained essentially constant after 3.65 h. The simulated groundwater head after 22 h was in close agreement with measured values at both sites, providing further confidence in the estimated seepage flux to the water table. The calibrated model from scenario D2 is used for all future analysis and comparisons.

### 3.5.3 Monte Carlo Sensitivity Analysis Results

Quantifying uncertainty in total seepage from the calibrated model (scenario D2) will be strongly influenced by the weighting, within and between each observation type (Eq. 3.9). For example, if the weight applied to the groundwater head data were higher than for the flood front flow (*ff* flow) and surface water stage, the total seepage would be larger (darker colors in Figure 3.8). Likewise, if groundwater head data weight was reduced or excluded, total seepage along the channel would be smaller. Therefore selecting the appropriate weights for the different datasets is vital during the calibration process. The weighting given in Eq. 3.9 means that, for example, when  $\phi = 0.3$  the model run output captured 70% of the variation in the observation data sets. For ease of discussion, an acceptable calibration result was selected as those model runs with a  $\phi \leq 0.3$  (see Table 3.4).

The calibrated model used all three data sets during the calibration process and provided a reasonable fit to *ff* flow, surface water levels, and groundwater head data. This is shown in Figure 3.8 for the six most informative parameters. Both the *ff* flow and surface water levels  $\phi$  are close to the optimal value (lowest  $\phi$  value), whereas the groundwater head  $\phi$  for the calibrated model was not the optimal objective value obtained during the uncertainty analysis. This may be a result of the influence of  $S_y$ ; the calibration will restrict  $S_y$  to close to the mean value (0 on the x axis) because the *ff* flow  $\phi$  will increase by more than an order of magnitude beyond this narrow range (Figure 3.8(j)). The model is unable to simultaneously optimize both objective functions (*ff* flow and *gwh*). Better groundwater head calibration results in a higher total seepage estimate (Figure 3.9), whereas a better

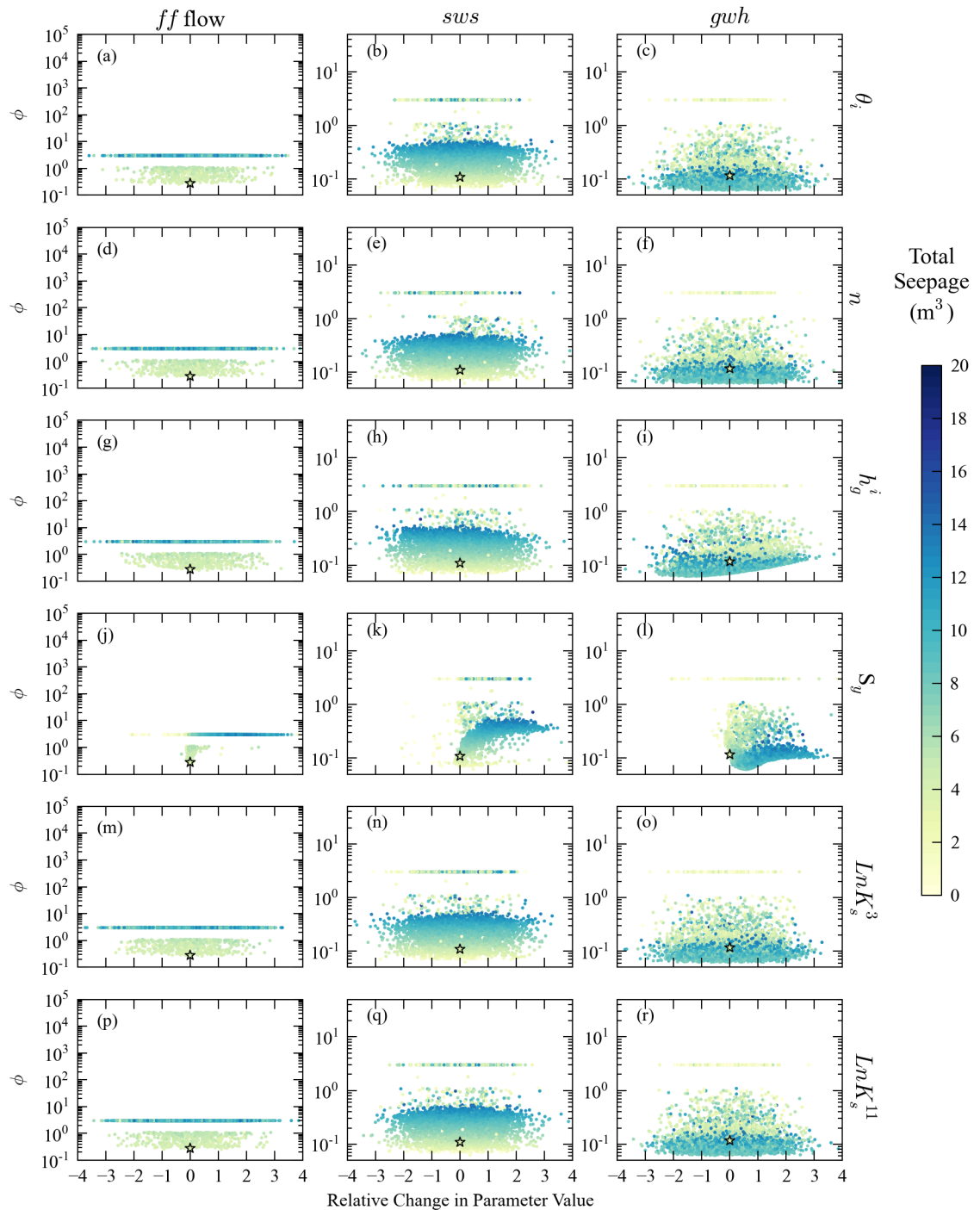


Figure 3.8: Six examples showing the impacts of changes in parameter value, expressed as given in standard deviations relative to the calibration model value, to the flood front flow (*ff flow*  $\phi$ ), surface water stage (*sws*  $\phi$ ), and groundwater head (*gwh*  $\phi$ ). Modeled parameter errors and values are provided in Tables 3.1 and 3.2. For example,  $\text{Ln}K_s^3$  equals  $-8.52$  ( $\text{m s}^{-1}$ )  $\pm 1$ ; therefore, when the number of  $\sigma$  equals  $-2, -0.5$ , and  $1$ ,  $\text{Ln}K_s^3$  equals  $-10.52, -9.02$  and  $-7.52$  respectively ((m), (n), and (o)). The color represents the total seepage flux ( $\text{m}^3$ ) along the channel. Stars represent the calibrated model  $\phi$  and total seepage flux.

$ff$  flow calibration results in a lower total seepage ( $7.09 \pm 2.03 \text{ m}^3$ ), the calibrated model is thus a compromise. For further discussion of the sensitivity analysis results displayed in Figure 3.8 and 3.9, refer to Appendix B.1, B.2, and B.3.

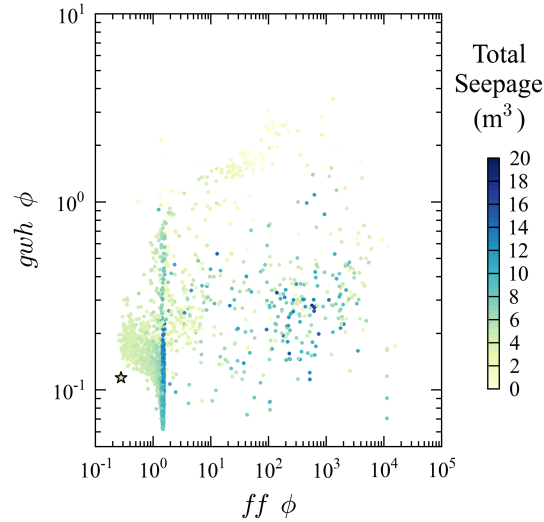


Figure 3.9: Flood front flow  $\phi$  versus the groundwater head  $\phi$ . The color represents the total seepage flux ( $\text{m}^3$ ) along the channel. Star represent the calibrated model  $\phi$ .

Approximately 90% of all Monte Carlo runs produced a groundwater head  $\phi \pm 0.3$ . This suggests that most of the modeled groundwater responses fit the observed data reasonably accurately. The relationship between groundwater head  $\phi$  and total seepage along the channel suggested that those model runs with a smaller error in groundwater head (e.g., lower groundwater head  $\phi$ ) tended to have higher total seepage ( $8.28 \pm 2.43 \text{ m}^3$ , Table 3.4). In comparison, 66% of all the surface water level  $\phi$  were less than 0.2. The total seepage for surface water level  $\phi \leq 0.2$  was  $7.09 \pm 2.03 \text{ m}^3$ , lower than the total seepage for groundwater head  $\phi \leq 0.2$ . Flood front data has previously been used to constrain this type of model (Shanafield et al., 2012); if the flood front data were the only dataset available for this study, total seepage would be estimated as  $4.09 \pm 0.04 \text{ m}^3$  (Table 3.4).

The average objective functions of the three output data sets for the six parameters are shown in Figure 3.10. The ideal result would be a localized area with a low objective function value (white/yellow zone) surrounded by higher objective function values. This would allow both the uncertainty in the parameter value and total seepage to be constrained. However, many of the individual parameters are not well constrained (width of

the white/yellow zone), with a range of  $\pm 3\sigma$  (e.g., Figure 3.10(a)). Only the range in specific yield values were constrained;  $\pm 0.2\sigma$  (Figure 3.10(d)). Based on the criterion that  $\bar{\phi} \leq 0.3$  represents a reasonable model, the range in total seepage was  $3.49 - 5.49 \text{ m}^3$  along the study reach, which compare favorably with the calibrated model total seepage of  $3.8 \text{ m}^3$ .

Table 3.4: Mean and variance of the total seepage ( $\text{m}^3$ ) along the channel for all Monte Carlo simulation results, and where  $\phi \leq 0.3$ .

	Total Seepage ( $\text{m}^3$ )	
	mean	variance
All $\phi$	7.92	7.54
<i>ff</i> flow $\phi \leq 0.3$	4.09	0.04
<i>sws</i> $\phi \leq 0.3$	7.09	4.10
<i>gwh</i> $\phi \leq 0.3$	8.28	5.90

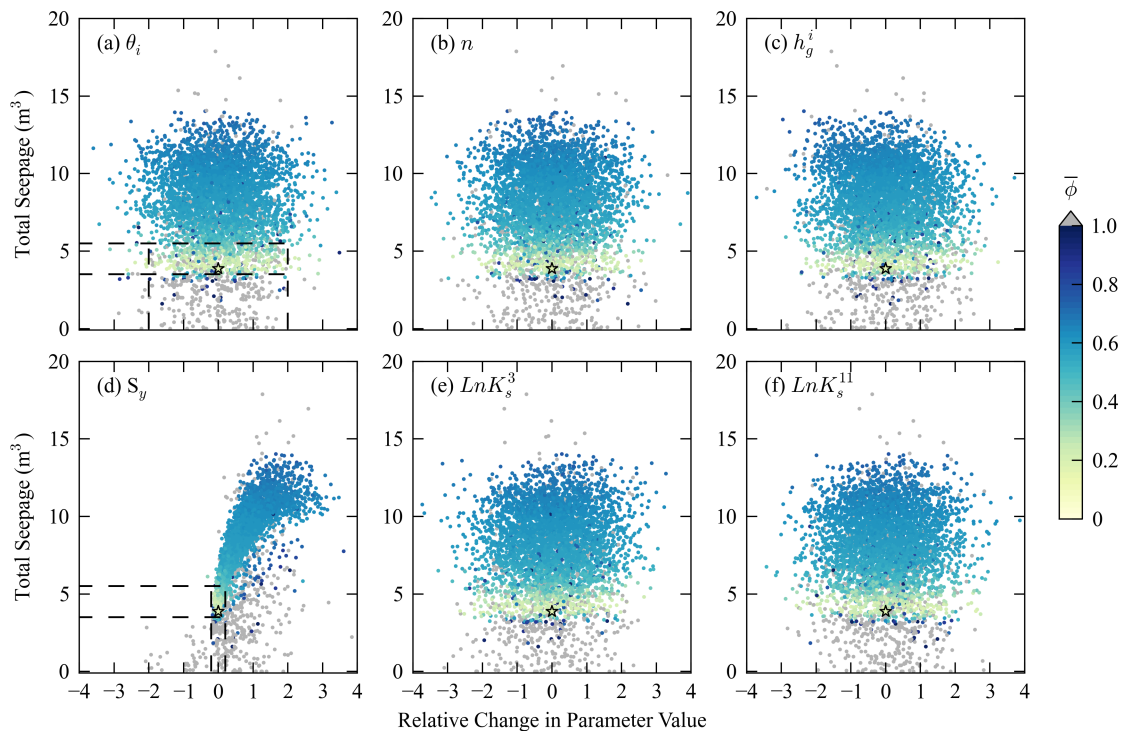


Figure 3.10: Uncertainty in total seepage flux ( $\text{m}^3$ ) from the study reach associated with changes in six parameter value (given in standard deviations,  $\sigma$ ) determined from the modified Monte Carlo analysis. The color represents the average  $\bar{\phi}$  of the three individual for each dataset shown in Figure 3.8. The star represents the total seepage flux and  $\bar{\phi}$  of the calibrated model.

## 3.6 Discussion

The longitudinal changes in seepage flux were estimated using a recently developed diffusion-wave model, capable of simulating stream flow events in channels with mild slope and backwater effects. The availability of surface water level and groundwater head data provided insight into the model's capacity to simulate and use this information to constrain the streambed hydraulic conductivity and seepage flux estimates along the reach. The inclusion of groundwater and surface water data estimated higher total seepage volumes than if the flood front data were used alone. The resultant calibrated model indicated longitudinal heterogeneity within the streambed sediments along the reach, enabling clear definition of areas of high and low seepage flux. A benefit of this approach is it results in a spatially integrated estimate of seepage flux rather than the need to upscale point measurements thereby capturing the sediment characteristics of the entire channel.

The seepage fluxes along the study reach vary by three orders of magnitude. A similar range of streambed conductivity – and by inference seepage flux – was observed by Kennedy et al. (2008) and Genereux et al. (2008) along 50-200 m stream sections in North Carolina. A recent study by Hatch et al. (2010) also identified a temporal variability of streambed seepage fluxes, as a result of deposition of sediment load during flow recession. This suggests that the simulated streambed seepage fluxes for the May 2011 Western Reflows Floodway flow event are unlikely to be exactly replicated in any subsequent flow event. Similarly, the reduced energy conditions associated with negative bed slopes would encourage deposition of finer, lower permeability sediments therefore bed slope will influence the spatial characteristics of streambed sediments.

The wet channel antecedent conditions have likely altered the influence that both surface water level and groundwater head will have on the model calibration (Table 3.2). The model uses the initial wetting up phase of the unsaturated zone to estimate streambed properties ( $K_s$ ). Therefore the initially wet channel conditions in this study would have limited the period in which the streambed properties could be estimated, thereby having a limited impact on the surface water level and a fast response in groundwater head (Niswonger et al., 2008; Shanafield et al., 2012). The relative importance of unsaturated zone

processes will increase where antecedent moisture conditions are drier and the depth to groundwater is greater.

The inclusion of Manning's  $n$  (scenario D3) did not improve the calibration suggesting the chosen distribution was an adequate approximation of the channel friction. Niswonger et al. (2008) showed that for the MODFLOW-SFR2 model the flood front timing is very sensitive to  $K_s$  where  $K_s$  values are greater than  $1.75 \text{ m d}^{-1}$ , but more sensitive to Manning's  $n$  when  $K_s$  is less than  $0.01 \text{ m d}^{-1}$ . This suggests that segments with low seepage fluxes (associated with low  $K_s$ ) are most sensitive to Manning's  $n$ .

The estimation of Manning's  $n$  is important because it helps control the flood front movement along the channel and the surface water level. For this study the influence of Manning's  $n$  on total seepage appears to be limited; however, previous studies have identified the difficulty and importance in the estimation of Manning's  $n$  (Khatibi et al., 2006). Because channel roughness has a strong control on shallow flow, the choice of Manning's  $n$  has significant impact on calibrating surface flow (Ackers, 1992; Hsu et al., 2006). In this study the same Manning's  $n$  distribution was applied to all of the 15 segments, negating any differences between segments; therefore, additional errors may have been incurred due to the spatial variability in Manning's  $n$  between segments. The presence of two bends in the study reach (Figure 3.2) and a slight increase in channel vegetation in the downstream segments would result in additional variability in the channel friction that was not captured (Jarrett, 1985). Further investigation should include this variability though to what extent this impacts model calibration is as yet unknown.

In the study channel, the depth to groundwater was shallow and the transition from unsaturated, disconnected to saturated, connected occurred rapidly; limiting the amount of information available with which to constrain the hydraulic conductivity of the streambed. However, where the depth to groundwater is greater, this transition would be slower and the groundwater response would assist in constraining the model. A possible limitation to the use of groundwater head data in this and future studies may also be the influence of localized heterogeneity in streambed sediments on the groundwater response. This could result in a localized groundwater response not representative of the average properties of the channel segment (Kennedy et al., 2010; Irvine et al., 2012).

To date, this model has only been applied to an artificial un-lined channel, however it has the potential to be applied to natural systems. The availability of LiDAR and remote sensing to characterize channel geometry (Passalacqua et al., 2012), in combination with data loggers that can be deployed to monitor surface flood movement and groundwater heads may enable catchment scale investigations. The main challenge associated with the use of this model in a natural system would be the adequate representation of the channel geometry and hydraulic properties, in particular the estimation of appropriate values for Manning's  $n$  roughness coefficient and the influence of vegetation on flow within the channel.

### **3.7 Conclusions**

The spatial variability of seepage flux beneath a 1387 m reach of artificial stream channel was successfully estimated using a numerical model that accounts for flood wave propagation at the surface, infiltration through the streambed and groundwater flow. We found that the method, which has previously only used flood front timing as a calibration constraint, provides more reliable seepage flux estimates when surface water level and groundwater head data are used in the calibration. For this study, surface water level and groundwater head data provided complementary information; lower total seepage estimates would have been estimated if this data were excluded. The total seepage for the study reach was estimated as  $4.2 \text{ m}^3$  with an uncertainty of  $\pm 0.6 \text{ m}^3$ , and the specific yield of the aquifer was shown to be the most influential parameter. Though a number of limitations have been highlighted in this study, the method offers promising opportunities to determine the longitudinal variability in seepage fluxes from ephemeral and intermittent streams.

### **Acknowledgments**

Funding for this research was provided by the National Centre for Groundwater Research and Training, an Australian Government initiative, supported by the Australian Research Council and the National Water Commission, and the Goyder Institute for Wa-

ter Research of South Australia. The authors would like to acknowledge Australian Blue Gums for allowing access and use of their land. We also acknowledge the field assistance provided by Nick White, Lawrence Burk, Louise Anders, Roger Cranswick, Mark De Jong and the staff from the Millicent office of South Australia Department of Environment, Water and Natural Resources. James McCallum provided assistance with PEST, and Dr. John Hutson with soil analysis. The authors wish to thank Graham Sander and three anonymous reviewers for comments that strengthened this work.



## Chapter 4

# Using sealed wells to measure water levels beneath streams and floodplains

Noorduijn, S.L., Cook, P. G., Wood, C. and White, N. (Submitted), Using sealed wells to measure water levels beneath streams and floodplains, Ground Water



## 4.1 Abstract

The design of wells beneath streams and floodplains has often employed tall stand pipes to prevent incursion of surface water into the well during flood events. Here, we present an approach to minimise the infrastructure demands in these environments, by sealing the well (e.g., prevent water entering the well) and monitoring the total pressure using a non-vented pressure transducer. We show that, whether the well is sealed or open to the atmosphere, the total pressure at a given depth in the aquifer will be equal to that within the well. The sealed well design was tested using a laboratory experiment where the total pressure responses were monitored in both an open and sealed well whilst the aquifer water level was varied. Pressure transducers were also used to record the air pressure within the head space of the sealed well and open well, and capacitance water level loggers recorded the actual water level in each well. The data recorded during the laboratory experiment showed that the responses in total pressure in both wells were identical. Therefore the water level in the aquifer can be obtained from the total pressure response in the sealed well corrected for any ambient changes in barometric fluctuation outside the well (not the head space air pressure). This indicates that the sealed well design is a viable alternative to tall stand pipes and also facilitates installation of wells beneath streams and floodplains.

## 4.2 Introduction

The construction of wells in or adjacent to streams and rivers has proven challenging due to the risk of inundation by surface water flows into the well. Inundation can generally be overcome by the construction of a tall standpipe that exceeds the height of any previously recorded flood events (see Figure 4.1). This prevents flood water from entering the well and artificially raising the groundwater level and changing water chemistry. However, this approach is costly, inconvenient, and still has the potential to be unsuccessful if surface water levels exceed the height of the standpipe.

Since the 1960s, electrical pressure transducers have been widely used in geotechnical engineering to determine pore water pressure in tailings dams and other structures



Figure 4.1: Wells with very tall standpipes are often constructed to avoid inundation by floodwaters. This example is from the Daly River, Australia (courtesy of Steven Tickell).

(Brooker et al., 1968; Gibson, 1963). Submersible electrical pressure transducers are now widely used to measure water level in wells, streams, rivers, and lakes (Freeman et al., 2004). Electrical pressure transducers record the total pressure above the sensor; within a groundwater well any change in water level will result in a proportional change in total pressure, assuming that barometric pressure remains constant.

In an unconfined shallow aquifer, the influence of barometric pressure on the water level can be significant and therefore needs to be accounted for when correcting such pressure data (Rasmussen and Crawford, 1997). Well design when using non-vented pressure transducers generally includes a vented cap to equalize the air pressure in the well to the ambient barometric pressure (Sprecher, 2008; USACE, 2005). Alternatively, vented pressure transducers have been designed to automatically compensate for changes in barometric pressure by connecting the reference pressure to the atmosphere, via a vent tube (Freeman et al., 2004). Such instruments are generally considered more accurate than the non-vented pressure transducers (Price, 2009). In an environment where inundation is likely to occur, installation of a vented pressure transducer is challenging. Maintaining the vent tube above the water level, either within the well or external to the well, may also prove to be a challenge.

Here we demonstrate that a sealed well, that is a capped and water tight, can be used to measure groundwater levels in an unconfined aquifer; this method of well construction can be used to monitor groundwater levels adjacent to/or beneath a stream or river, negating the need for excessively tall standpipes. A laboratory experiment was conducted whereby a sealed and unsealed well were constructed in a container representing an aquifer. This allowed the water level to vary and the response in the sealed well and unsealed well to be monitored.

### 4.3 Theory

The assumption in the use of a non-vented pressure transducer is that the total pressure recorded at the measurement point within the well is equal to the total pressure within the aquifer at the same depth. In an unsealed well (i.e., the water level in the well is affected by the ambient barometric fluctuations) in an unconfined aquifer, the total pressure recorded is:

$$P_T = P_W + A \quad (4.1)$$

where  $P_T$  is the total pressure ( $\text{kg m}^{-1} \text{s}^{-2}$ ),  $P_W$  is the pressure exerted by the overlying water column ( $\text{kg m}^{-1} \text{s}^{-2}$ ), and  $A$  is the ambient barometric pressure measured in the well column above the water level ( $\text{kg m}^{-1} \text{s}^{-2}$ ). Assuming that the total pressure recorded by the pressure transducer in the sealed well is equal to the total pressure in the aquifer, the water pressure in the aquifer can be obtained by correcting the total pressure from a sealed well with the ambient barometric pressure measurements (see Figure 4.2):

$$P_W^O = P_T^S + A^O \quad (4.2)$$

where  $P_W^O$  is the pressure exerted by the overlying water column in the aquifer ( $\text{kg m}^{-1} \text{s}^{-2}$ ),  $P_T^S$  is the total pressure recorded by a submerged pressure transducer in a sealed well ( $\text{kg m}^{-1} \text{s}^{-2}$ ), and  $A^O$  is the ambient barometric pressure measured ( $\text{kg m}^{-1} \text{s}^{-2}$ ). The water pressure can then be converted to water level if the water density is known. By sealing the well the groundwater level response is dampened, due the limited compressibility of the air within the well, when the groundwater level in the surrounding aquifer

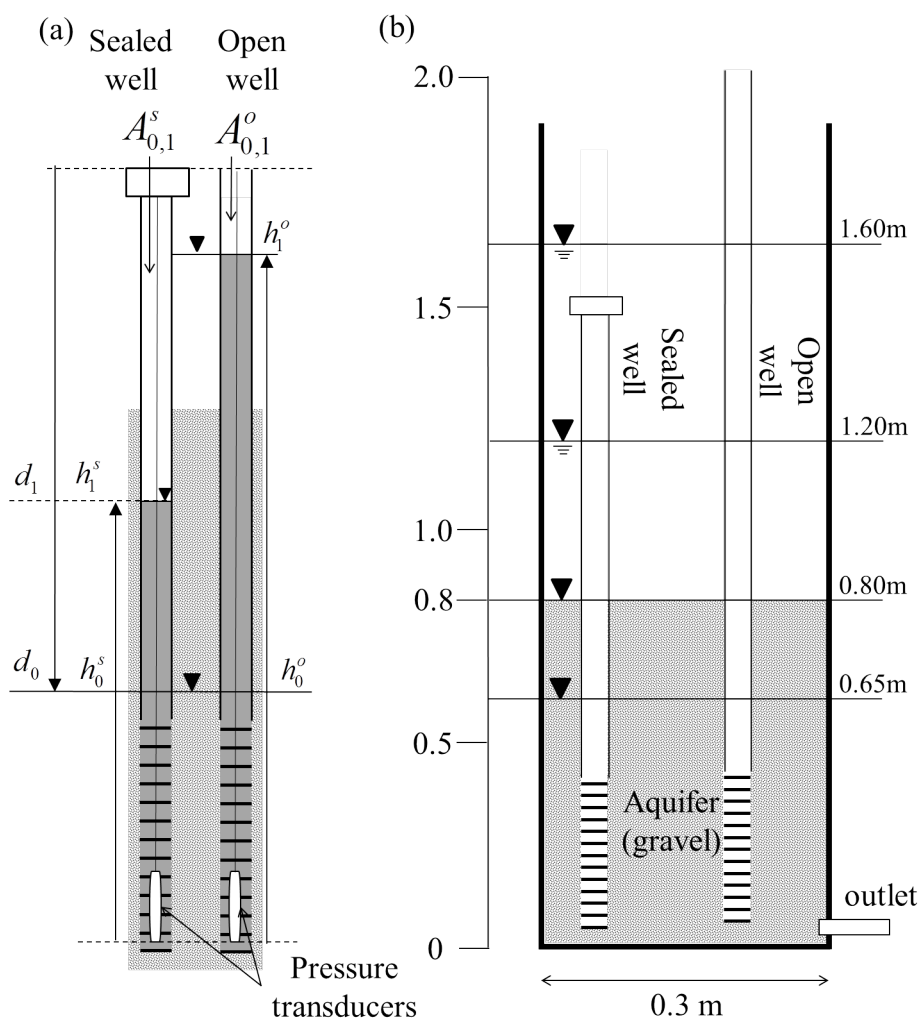


Figure 4.2: Schematic representation of (a) a sealed well and the measurements involved in calculating the hydraulic head using a non-vented pressure transducer and (b) the experimental setup with the experiments water levels are indicated. All groundwater levels ( $h^O$  and  $h^S$  for the open and sealed well respectively) are relative to the measurement point (i.e., location of the pressure transducer sensor) and all depth measurements refer to the sealed well ( $d_0$  and  $d_1$ ) and are relative to the top of casing.

rises. Suppose that two wells have screens at the same depth in the aquifer. Then suppose that one of two wells was sealed and then either  $P_W$  or  $A$  increased. Initially, the water pressure in the open well will equal that of the sealed well ( $P_{W,0}^O = P_{W,0}^S = P_{W,0}$ ); similarly for the overlying air pressure ( $A_0^O = A_0^S = A_0$ ). In the following we use superscript  $O$  and  $S$  to represent the open (unsealed) and sealed wells, and subscript 0 and 1 to represent time with 0 being the initial conditions. An increase in either the barometric air pressure or water level will result in an increase in total pressure in the aquifer and within the screened interval in both wells. A schematic representation of the groundwater level response in a sealed well, as a result of a rise in groundwater level in the aquifer from  $h_0^O$  to  $h_1^O$  is shown

in Figure 4.2(a). The change in total pressure response in the sealed well will be equal to that observed in an open well:

$$\Delta A^O + \Delta P_W^O = \Delta A^S + \Delta P_W^S \quad (4.3)$$

Within the sealed well an increase in total pressure is expressed as an increase in the air pressure and the dampened groundwater rise. This pressurization of the air column can be described by Boyle's gas law:

$$A_0^S V_0 = A_1^S V_1 \quad (4.4)$$

where  $V_0$  and  $V_1$  are the volume of the air column in the sealed well prior to and after a change in air pressure and groundwater level ( $\text{m}^3$ ). The corresponding groundwater rise within the sealed well can be described as:

$$d_0 + h_0^S = d_1 + h_1^S \quad (4.5)$$

$$\frac{V_0}{\pi r^2} + \frac{P_{W,0}^S}{\rho g} = \frac{V_1}{\pi r^2} + \frac{P_{W,1}^S}{\rho g} \quad (4.6)$$

where  $\frac{V}{\pi r^2} = d$  is the length of the air column (m),  $r$  is the radius of the well (m),  $\frac{P_{W,0}^S}{\rho g} = h^S$  is the length of the water column (m),  $\rho$  is the density of water ( $\text{kg m}^{-3}$ ) and  $g$  is gravitational acceleration ( $\text{m s}^{-2}$ ) (Figure 4.2(a)). The groundwater pressure head within the sealed well can therefore be expressed by rearranging Eq 4.3 and substituting in Eq 4.4, and 4.6:

$$P_{W,1}^S = A_1^O + P_{W,1}^O - \left( \frac{A_0^S V_0}{V_0 + \left( \frac{P_{W,0}^S}{\rho g} - \frac{P_{W,1}^S}{\rho g} \right) \pi r^2} \right) \quad (4.7)$$

## 4.4 Methodolgy

### 4.4.1 Laboratory setup

To examine the applicability of using sealed wells, a laboratory experiment was set up to compare the total pressure recorded by non-vented pressure transducers in open and sealed wells. Additional instrumentation examined the relative change in water level within the wells during the experiment.

Two PVC wells (PN 18) were constructed with 300 mm screened sections. A barrel union (50 mm, AS/NZS 1477, PN 18 PVC) was used to seal one of the wells; these are readily available at hardware shops and pool suppliers. The open well remained uncapped during the entire experiment. The wells were installed in a container (dimensions were 1.92 m high and 0.3 m radius), sealed at bottom to form a ‘bucket’. Coarse gravel was used as the aquifer material, which supported the wells and maintained the stability of the container. An outlet tap was installed at the base of the container to allow water to drain.

Each well contained: 1) an Odyssey Capacitance water level recorder used to monitor the actual water level within the well, 2) non-vented pressure transducers (In-Situ Inc LevelTROLL® 300 Series,  $\pm 0.2\%$  accuracy) to record the total pressure (i.e., the pressure exerted by the overlying water column and air), and 3) barometric pressure transducer (In-Situ Inc. BaroTROLL®,  $\pm 0.05\%$  accuracy) to record the changes in air pressure within each well. The density and salinity of the water was  $1.0 \text{ g cm}^{-3}$  and  $425 \mu\text{S cm}^{-1}$  respectively. All pressure measurements are reported as meters of water ( $\text{m H}_2\text{O}$ ). All instrumentation was set to record data on 1 min intervals. The length of the capacitance water level recorders used was 1 m for the sealed well, and 3 m for the open well, total pressure transducers were suspended in the screened sections of the wells.

### 4.4.2 Experimental design

All instrumentation was installed within both wells and the sealed well was sealed (via the barrel union) prior to the addition of water to the container. The initial water level was below the top of the screens in both wells.

The water level within the container was then raised in stages and the changes in total

pressure, water level, and air pressure within the wells were monitored (Figure 4.2(b)). A series of step increases in water level were applied, in addition to an attempt to replicate the rising and recessive limbs of a stream hydrograph. The container was filled with water to 0.65 m above the base from 0.0-0.04 days and maintained for 5 hrs (0.04-0.2 days). The water level was then increased to 0.8 m (0.20-0.24 days) and maintained for a period of 15hrs (0.24-1.08 days). For the last step increase the water level was raised to 1.2 m from 1.08-1.29 days, and maintained for 12 hrs (1.29-1.8 days). In the final part of the experiment, the water level increased to 1.6 m (1.8-2.17 days), after maintaining this water level for 2.4 hrs (mimicking a flood event), the container was allowed to drain under gravity (using the outlet at the base of the container) to a water level of 0.58 m. This water level was maintained for 10 days.

## 4.5 Results

There was no measurable difference between the total pressure in the sealed well and that recorded in the open well; any differences were within the error of the instruments (Figure 4.3(a)). In contrast, the actual water level (determined from the capacitance water level loggers) in the open and sealed wells is quite different (Figure 4.3(b)). The response of the water level in the sealed well started to deviate from the open well, when the initial water level was increased above the screened section of the well, i.e., above 0.4 m. The increase in water level in the sealed well was dampened due to the limited compressibility of the trapped air. During subsequent step increases in water level, the water level in the sealed well rose during periods when the level in the open well was stable, this was most apparent between 1.29-1.8 days. In combination with a decrease in barometric pressure within the sealed well, this indicates that the barrel union was not airtight. This was also apparent during the final part of the experiment, after the water level was raised and lowered. If the barrel union were airtight, the water level in the sealed well would remain constant once the water level in the open well was stable (i.e., after 2.3 days); however the water level slowly declined until it was equal to that of the open well.

The rapid decline in surface water stage in the container at 2.3 days resulted in the air pressure in the sealed well being less than the ambient air pressure; a hanging water

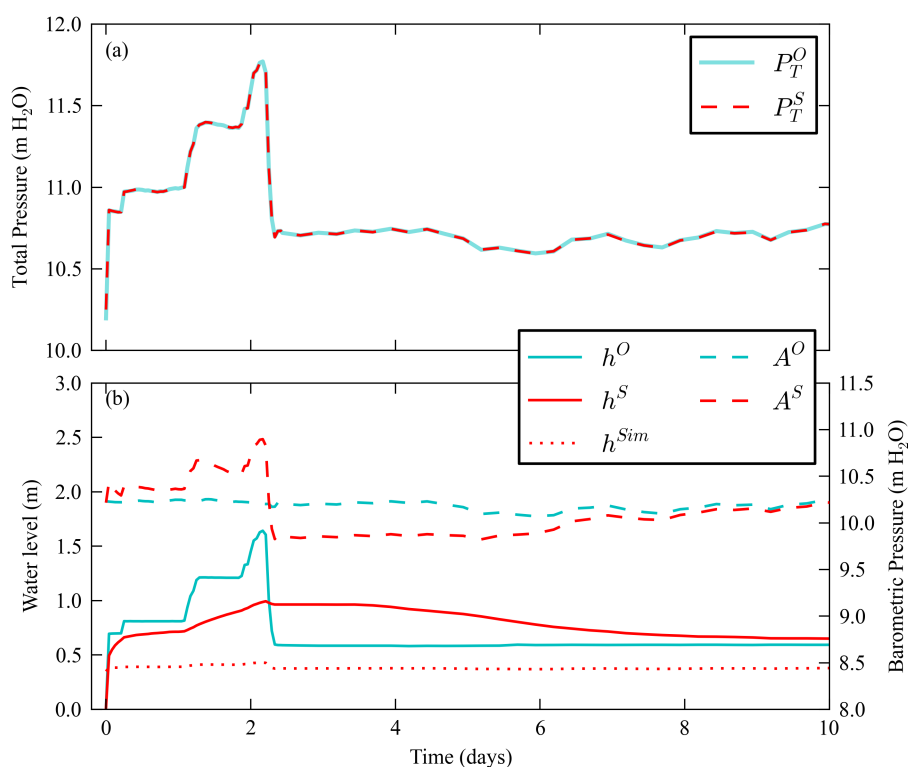


Figure 4.3: Observed response to the three level changes in the pressure transducers and capacitance probes within the open and sealed wells. (a) shows the total pressure from the non-vented pressure transducer located in the screened section of the open ( $P_T^O$ ) and sealed ( $P_T^S$ ) wells, expressed as length (m H<sub>2</sub>O). (b) shows the actual water level response monitored by the capacitance water level loggers in the open ( $h^O$ ) and sealed ( $h^S$ ) wells. The water level response in a theoretical airtight, sealed well for this experiment (calculated using Eq 3.7) is also shown ( $h^{Sim}$ ). The barometric pressure is also shown for the open (i.e., ambient barometric pressure) ( $A^O$ ) and sealed ( $A^S$ ) well, expressed as length (m H<sub>2</sub>O).

column had formed within the sealed well (e.g., water level in the sealed well was higher than the open well). The leaky barrel union slowly allowed the air pressure to equalize with the ambient barometric pressure which allowed the water level to drop. The water level response in a fully sealed well calculated using Eq 3.7 is shown in Figure 4.3(b). The results indicated that the maximum change in water level would not exceed 0.1 m above the top of the screens; this is significantly smaller than that observed in the laboratory test.

The barrel union was tested to check whether water could enter the well if the air pressure within the sealed well was below the ambient barometric pressure and the sealed well was submerged. This was achieved by submerging the barrel union whilst the sealed well was depressurized (described above). The results suggested that the barrel union was water tight but not airtight, however this had no impact on the total pressure response in the sealed well (Figure 4.3(a)). This indicates that an air tight seal is not necessary, but a

water tight seal is. A standard class 18 PVC push-cap was also included in the experiment; however the cap was unable to prevent the inflow of surface water into the well i.e., it was neither water nor air- tight. Other methods, such as the use of silicon to seal the push- cap, may be used however further testing would be required.

## 4.6 Discussion

This study has demonstrated that the total pressure recorded by a non-vented pressure transducer in a sealed well is equal to that recorded in an open well. Therefore, assuming that the ambient barometric pressure is also monitored, the water level within the aquifer can be obtained by correcting this total pressure for barometric fluctuations (Freeman et al., 2004).

This method of well completion will permit the installation of wells in stream and river beds, enabling direct monitoring of the connection state of intermittent and ephemeral streams (Brunner et al., 2009; Post and Von Asmuth, 2013). Obtaining field observations of the connection state of a stream has proven a challenge, requiring a significant amount of instrumentation (tensionmeters, manometers, and other similar devices) and infrastructure (e.g. Dahan et al., 2007). Similarly the need for tall stand pipes can be avoided; the well can be constructed such that the stand pipe height is at or near the streambed level thereby reducing the destructive impact of debris during flow events which might otherwise destroy a well within the stream or on a river floodplain.

The assumption in the application of this well design is that any change in barometric pressure is instantaneously transferred to the water level within the aquifer (i.e., barometric efficiency = 1) (Rasmussen and Crawford, 1997; Spang, 2002). This is typically the case in shallow unconfined aquifers. As the water table depth increases, the transmission of atmospheric pressure through the vadose zone is effected by the vertical permeability, moisture content and soil gas compressibility within this zone (Weeks, 1979). The resulting delay in water level response would need to be considered when correcting the total pressure data. In such cases the barometric efficiency would need to be checked routinely.

A similar well construction method has been applied to artesian wells for many years. Where the potentiometric water level is in excess of 2 m above ground level, the need for

tall standpipes is generally overcome by sealing the well at a manageable height above ground level, and monitoring the potentiometric water level using a pressure gauge at the well head (Logani, 1985; Rogers and Moore, 1997; Alfortish et al., 2012).

Our experiment has also shown that the need for a perfect seal (e.g., both air and water tight) is not necessary. In terms of total pressure, incursion of surface water into the well is only an issue where the rate of inflow is greater than the rate at which the water can be dissipated into the aquifer. Where this is the case, the total pressure within the sealed well will be unaffected. Incursion of surface water into the well will have an impact on the groundwater chemistry; therefore a water tight seal will provide the most reliable data. Alternative capping options have been developed that form a complete seal, e.g., Hubbell et al. (2004). However, such caps are costly and not widely available.

The manual water level measurements needed to convert the recorded total pressure to a reference height requires consideration. To obtain the manual measurement using a dip meter, the cap must be removed which will mean  $A^S$  becomes  $A^O$ , and may result in either a rise or fall in the water level within the well due to pressure equalization with the pressure in the aquifer; the total pressure will be unaffected. It would be necessary to monitor the water level until it stabilized before taking the reading; an estimate of this time may be obtained by observing the water level response in the well to a slug test (Butler, 2005).

Water chemistry samples can either be obtained as grab sample for laboratory analysis or time series data using multi-parameter instruments within the well (e.g., the AquaTroll 400 will record  $Ec$ ,  $pH$ ,  $DO$ , temperature and water pressure within the well). Both approaches require that the cap be removed from the sealed piezometer to sample the water or install the required instrumentation. When installing water chemistry instrumentation within the well, the sensors will need to be located within the screened section of the well to encounter active flow. The water will flow through the well screens uninhibited, therefore sealing the well will not impact the water chemistry in this area of the well.

We have also demonstrated that knowing the water level change in a sealed well is not useful. The use of vented pressure transducers for this well completion would pose a similar issue to the use of tall stand pipes, i.e., the vent tube would need to be connected to

the atmosphere, and the debris carried by a flow event may damage the vent tube. Hubbell et al. (2004) describe a technique whereby a differential pressure transducer is vented in the head space of the sealed well. However this would result in monitoring the water level in the sealed well, rather than the aquifer. The ability of this sealed well design allows both the collection of hydraulic head data and chemistry data, such as electrical conductivity, making it an improvement on current stand pipe design.

## **4.7 Conclusion**

The potential for inundation of the well casing from surface water has led to the use of tall standpipe structures for wells near large rivers. We have shown that a feasible and cost effective alternative is sealing a well coupled with the use of non-vented pressure transducers to monitor the total pressure. A laboratory experiment simulated a rise in water level above the top of the sealed well to determine the impact on the total pressure within the well. This has clearly shown that the total pressure recorded in a sealed well is equal to that of an open well. Similarly, in combination with barometric data, the aquifer water level response can be obtained from the total pressure response in a sealed well. The experiment has also indicated that the seal needs to be water tight, rather than air tight. Therefore, the use of sealed wells in environments where inundation will occur is a viable well completion design.

## **Acknowledgments**

Funding for this research was provided by the National Centre for Groundwater Research and Training, an Australian Government initiative, supported by the Australian Research Council and the National Water Commission, and the Goyder Institute for Water Research of South Australia. We also acknowledge the assistance provided by Dr Mark Trigg.

# Chapter 5

## Conclusions

### 5.1 Overview

This doctoral research has explored the use of different hydraulic methods to estimate spatial variability in surface water – groundwater exchange fluxes along both gaining and losing streams. This was accomplished by addressing the three main aims:

1. *to determine the representative scale at which standard hydraulic methods can be applied in this field of research.*

Prior application of Darcy's law for determining groundwater discharge to a stream assumes that the discharge estimate is an accurate representation of groundwater discharge along significant reaches of a stream (or until the next available data point). This research has found that the length of stream over which the discharge estimate occurs is closely related to the distance between the observation well (used to compute hydraulic gradient) and the stream. For example, a groundwater discharge estimate obtained using Darcy's law and a well at a distance of 50 m from the stream will represent discharge occurring along approximately 50 m of the stream. This work has demonstrated the need to acknowledge and incorporate the scale limitations of the approach.

2. *to quantify the variability in surface water – groundwater fluxes in ephemeral environments*

The spatial variability in seepage flux along a 1000 m-long, initially-dry, artificial drainage channel was estimated using a combined field and numerical modelling approach. In this work we examine how the inclusion of additional hydraulic data (i.e.,

surface water level, groundwater level) into the model calibration process was examined. The research found that the inclusion of groundwater level data provided additional constraints during the calibration process, which ultimately improved the estimates of seepage flux. Hence, there are significant benefits to capturing the groundwater response to a flow event, particularly beneath the streambed. In addition, the sensitivity and uncertainty of the model was explored; the results of which suggest that alongside obtaining an accurate estimate of the specific yield of the aquifer, Manning's  $n$  and channel geometry are very important. A benefit of this approach is that a significant proportion of the data required can be obtained by deploying automated sensors in and beneath the channel.

### *3. to develop methods of measuring hydraulic heads beneath and adjacent to streams*

This research has demonstrated, through controlled laboratory experiments, that by sealing piezometers (i.e., capped and water tight) it is possible to capture the groundwater response to extreme flow events even when the piezometers are inundated. Although similar well completion methods are employed for artesian wells, no previous research has been conducted into the application of sealed wells within streambeds. The use of total pressure transducers enables this well completion technique to be a viable alternative to conventional, more expensive options. This work has implications for obtaining groundwater level data in both losing and gaining streams.

These findings will contribute to the application of hydraulic data in natural environments, thereby leading to a better understanding and quantification of surface water – groundwater fluxes.

## **5.2 Future work**

This research has brought to light a number of possible avenues for future research. A better understanding of the spatial limitations of methods applied to estimate surface water - groundwater fluxes may aid up- and down scaling. An extensions to the work conducted in Chapter 2 would involve the use of 3D modelling of a similar change in stage level. Determining the impact of aquifer properties on the current 2D model is limited to

those wells at  $x > 20$  m from the stream (two aquifer thicknesses from the stream). This is due to the influence of both vertical and horizontal flow path close to the stream which are not accounted for in a 2D model. The use of a 3D model would enable investigation of the influence of aquifer properties on estimating groundwater discharge close to the stream ( $x < 20$  m). In addition to this, the application of alternative approaches to generating stochastic K-fields i.e., the use of training images and multiple-point statistics (Mariethoz et al., 2010; Mariethoz and Kelly, 2011). An important extension of the work described in Chapter 3 would be the application of the diffusion-wave model (Shanafield et al., 2012) on a natural stream or river. At present this model has only been used on artificial channels, its implementation in a catchment scale model may also prove interesting. It is likely that in applying this numerical code to a natural system, the sensitivity of the input parameters to the flood front timing would alter. This would provide greater insight into parameter importance. For example, natural systems are rarely straight flat channels therefore obtaining an accurate estimate of Manning's  $n$  could become important when building the model (see Appendix B.4 for further discussion). Similarly, where the depth to groundwater is large (i.e.,  $> 15$  m bgl), accurately capturing the unsaturated zone properties of both the streambed sediments and aquifer will be essential. A natural follow on from the work described in Chapter 4, would be the instrumentation of sealed wells in the field, similar to work conducted by Schmidt et al. (2012). The laboratory study forms a foundation for the theoretical understanding of hydraulics and provides information on the key features of the design of such a well; i.e., a water-tight seal is necessary as a minimum requirement. The installation of a sealed well in the field would provide an additional proof of concept for this design. The data collected by this approach may then be applied to numerical models similar to (Shanafield et al., 2012) to enhance our ability to estimate seepage fluxes and therefore groundwater recharge.



# Bibliography

- Abdulrazzak, M. J., 1983: Recharge from ephemeral streams following wetting front arrival to water table. *Water Resour. Res.*, **19** (1), 194–200.
- Ackers, P., 1992: Hydraulic design of two-stage channels. *Proc. Inst. Civil Eng.-Water Maritime Energy*, **96** (4), 247–257.
- Alfortish, M., T. Brandon, R. Gilbert, T. Stark, and J. Westerink, 2012: *Geotechnical Reconnaissance of the 2011 flood on the Lower Mississippi River, Report No. GEER-029*. Geotechnical Extreme Events Reconnaissance Association.
- Barlebo, H. C., M. C. Hill, and D. Rosbjerg, 2004: Investigating the macrodispersion experiment (MADE) site in Columbus, Mississippi, using a three-dimensional inverse flow and transport model. *Water Resour. Res.*, **40**, W04211, doi:10.1029/2002WR001935.
- Barlow, P. M., L. A. DeSimone, and M. A. F., 2000: Aquifer response to stream-stage and recharge variations. ii. convolution method and applications. *J. Hydrol.*, **230**, W04211, doi:10.1016/s0022-1694(00)00176-1.
- Battle-Aguilar, J. and P. G. Cook, 2012: Transient infiltration from ephemeral streams: a field experiment at the reach scale. *Water Resour. Res.*, **48** (11), doi:10.1029/2012WR012009.
- Bear, J., 1972: *Dynamics of Fluid Flow in Porous Media*. Dover Publishing, New York.
- Birkhead, A. L. and C. S. James, 2002: Muskingum river routing with dynamic bank storage. *J. Hydrol.*, **264**, 113 – 132, doi:10.1016/S0022-1694(02)00068-9.
- Blasch, K., T. P. Ferré, J. Hoffmann, D. Pool, M. Bailey, and J. Cordova, 2013: Processes controlling recharge beneath ephemeral streams in southern arizona. *Groundwater Recharge in a Desert Environment: The Southwestern United States*, J. F. Hogan, F. M.

- Phillips, and B. R. Scanlon, Eds., American Geophysical Union, Washington, D. C., 23–58, doi:10.1029/009WSA05.
- Blöschl, G., 2001: Scaling in hydrology. *Hydro. Proc.*, **15** (4), 709 – 711, doi: 10.1002/hyp.432.
- Brooker, E. W., J. S. Scott, and P. Ali, 1968: Research Notes: A Transducer Piezometer for Clay Shales. *Canadian Geotech. J.*, **5** (4), 256–264.
- Brooks, R. H. and A. T. Corey, 1964: Hydraulic properties of porous media. *Hydrology Papers*, **24**.
- Brunner, G. W., 2010: *HEC-RAS, river analysis system user's manual, version 4.1*. U.S. Army Corps of Engineers, Hydrological Engineering Center (HEC), Davis, CA.
- Brunner, P., C. T. Simmons, and P. G. Cook, 2009: Spatial and temporal aspects of the transition from connection to disconnection between rivers, lakes and groundwater. *J. Hydrol.*, **376** (1-2), 159–169, doi:10.1016/j.jhydrol.2009.07.023.
- Butler, J. J., 1990: The role of pumping tests in site characterization - some theoretical considerations. *Ground Water*, **28** (3), 394 – 402, doi:10.1111/j.1745-6584.1990.tb02269.x.
- Butler, J. J., 2005: Hydrogeology methods for estimation of hydraulic conductivity. *Hydrogeophysics*, Y. Rubin and S. Hubbard, Eds., Springer, 23–58.
- Callegary, J. B., J. M. Leenhouts, N. V. Paretto, and C. A. Jones, 2007: Rapid estimation of recharge potential in ephemeral-stream channels using electromagnetic methods, and measurements of channel and vegetation characteristics. *J. Hydrol.*, **344**, 17 – 31, doi: 10.1016/j.jhydrol.2007.06.028.
- Camacho, E., C. Pérez-Lucena, J. Roldán-Cañas, and M. Alcaide, 1997: IPE: Model for management and control of furrow irrigation in real time. *J. Irrig. Drainage*, **123**, 264 – 269, doi:10.1061/(asce)0733-9437(1997)123:4(264).

- Chenini, I. and A. Ben Mammou, 2010: Groundwater recharge study in arid region: An approach using GIS techniques and numerical modeling. *Comp. and Geosc.*, **36**, 801 – 817, doi:0.1016/j.cageo.2009.06.014.
- Chow, V., 1959: *Open Channel Hydraulics*. McGraw-Hill, New York, USA.
- Chow, V., D. R. Maidment, and L. W. Mays, 1988: *Applied Hydrology*. McGraw-Hill, New York, USA.
- Conant Jr, B., 2004: Delineating and Quantifying Ground Water Discharge Zones Using Streambed Temperatures. *Ground Water*, **42 (2)**, 243 – 257.
- Constantz, J., 2008: Heat as a tracer to determine streambed water exchanges. *Water Resour. Res.*, **44**, doi:10.1029/2008wr006996.
- Cook, P. G., S. Lamontagne, D. Berhane, and J. F. Clarke, 2006: Quantifying groundwater discharge to Cockburn River, southeastern Australia, using dissolved gas tracers  $^{222}\text{Rn}$  and  $\text{SF}_6$ . *Water Resour. Res.*, **42**, W10411, doi:10.1029/2006WR004921.
- Copt, N. and A. Findikakis, 2004: Stochastic analysis of pumping test drawdown data in heterogeneous geologic formations. *J. Hydraul. Res.*, **42 (2)**, 59 – 67.
- Cushman, J. H., 1986: On Measurement, Scale, and Scaling. *Water Resour. Res.*, **22 (2)**, 5W4044, doi:10.1029/WR022i002p00129.
- Dagan, G., 1997: Stochastic modelling of flow and transport: The broad perspective. *Subsurface Flow and Transport*, G. Dagan and S. Neuman, Eds., Cambridge Univ. Press, New York, 3 – 19.
- Dahan, O., Y. Shani, Y. Enzel, Y. Yechieli, and A. Yakirevich, 2007: Direct measurements of floodwater infiltration into shallow alluvial aquifers. *J. Hydrol.*, **344**, 157 – 170, doi: 10.1016/j.jhydrol.2007.06.033.
- Dahan, O., R. Talby, Y. Yechieli, E. Adar, N. Lazarovitch, and Y. Enzel, 2009: In Situ Monitoring of Water Percolation and Solute Transport Using a Vadose Zone Monitoring System. *Vadose Zone J.*, **8**, 916 – 925, doi:10.2136/vzj2008.0134.

- Dahan, O., B. Tatarsky, Y. Enzel, C. Kulls, M. Seely, and G. Benito, 2008: Dynamics of flood water infiltration and ground water recharge in hyperarid desert. *Ground Water*, **46**, 450 – 461, doi:10.1111/j.1745-6584.2007.00414.x.
- Darcy, H. P. G., 1856: *Les fontaines publiques de la ville de Dijon (The public fountains of the city of Dijon)*. Victor Dalmont, Paris.
- Deutsch, C. V. and A. G. Journel, 1998: *GSLIB Geostatistical Software Library and User's Guide, 2nd Ed.* Oxford University Press, New York.
- Doble, R., P. Brunner, J. McCallum, and P. G. Cook, 2012: An analysis of river bank slope and unsaturated flow effects on bank storage. *Ground Water*, **50**, 77 – 86, doi:10.1016/j.jhydrol.2008.12.018.
- Doherty, J., 2010: *PEST Model Independant Paramater Estimation*. Watermark Numerical Computing, Brisbane, Australia.
- Eaton, T., 2006: On the importance of geological heterogeneity for flow simulation. *Sediment. Geol.*, **184 (3-4)**, 187 – 201, doi:10.1016/j.sedgeo.2005.11.002.
- Fariclough, M. C., 2010: *Coompana 1:250 000 Geology map sheet SH 52-15*. Geological Survey of South Asutralia.
- Fawcett, R. G. and N. Collis-George, 1967: A filter paper method for determining the moisture characteristic of soil. *Aust. J. Exp. Agric. Anim. Husb*, **7**, 162 – 167.
- Fleckenstein, J. H. and G. E. Fogg, 2008: Efficient upscaling of hydraulic conductivity in heterogeneous alluvial aquifers. *Hydrogeol. J.*, **16**, 1239–1250, doi:10.1007/s10040-008-0312-3.
- Fleckenstein, J. H., R. Niswonger, and G. E. Fogg, 2006: River-aquifer interactions, geological heterogeneity, and low-flow management. *Ground Water*, **44 (6)**, 837 – 852, doi:10.1111/j.1745-6584.2006.00190.x.
- Freeman, L. A., M. C. Carpenter, D. O. Rosenberry, J. P. Rousseau, R. Unger, and J. S. McLean, 2004: Use of submersible pressure transducers in water-resource investiga-

- tions, chap. a3. *Techniques of Water-Resources Investigation*, U. S. Geol. Sur., Reston, VA.
- Freeze, R. and J. Cherry, 1979: *Groundwater*. Prentice-Hall, Sydney.
- Genereux, D. P., S. Leahy, H. Mitasova, C. D. Kennedy, and D. R. Corbett, 2008: Spatial and temporal variability of streambed hydraulic conductivity in West Bear Creek, North Carolina, USA. *J. Hydrol.*, **358**, 332 – 353, doi:10.1016/j.jhydrol.2008.06.017.
- Gibson, R. E., 1963: An Analysis of System Flexibility and its Effect on Time-Lag in Pore-Water Pressure Measurements. *Geotechnique*, **13**, 1–11.
- Gleeson, T., K. Novakowski, P. Cook, and T. Kyser, 2009: Constraining groundwater discharge in a large watershed: Integrated isotopic, hydraulic, and thermal data from the Canadian shield. *Water Resour. Res.*, **45**, W08402, doi:10.1029/2008wr007622.
- Gomez-Hernandez, J. J. and S. M. Gorelick, 1989: Effective groundwater model parameter values: Influence of spatial variability of hydraulic conductivity, leakance and recharge. *Water Resour. Res.*, **25** (3), 405–419, doi:10.1029/WR025i003p00405.
- Goodrich, D. C., et al., 2004: Comparison of methods to estimate ephemeral channel recharge, Walnut Gulch, San Pedro River Basin, Arizona. *Ground-water recharge in desert environments: The Southwestern United States*, J. Hogan, F. Phillips, and B. Scanlon, Eds., American Geophysical Union, Washington, D.C., 77 – 100.
- Greacen, E. L., G. R. Walker, and P. G. Cook, 1989: Evaluation of the filter paper method for measuring soil water suction. *International meeting at University of Utah on measurement of soil and plant water status*, 137 – 145, 1.
- Hall, F. R. and A. F. Moench, 1972: Application of convolution equation to stream-aquifer relationships. *Water Resour. Res.*, **8** (2), 487–493, doi:10.1029/WR008i002p00487.
- Hameed, T., M. A. Marino, and M. N. Cheema, 1996: Time series modeling of channel transmission losses. *Agric. Water Manage.*, **29**, 283 – 298, doi:10.1016/0378-3774(95)01201-x.

- Hantush, M. M., 2005: Modeling stream-aquifer interactions with linear response functions. *J. Hydrol.*, **311**, 59–79, doi:10.1016/j.jhydrol.2005.01.007.
- Harbaugh, A. W., 2005: *MODFLOW-2005, The U.S. Geological Survey modular groundwater model – the Ground-Water Flow Process*. U.S. Geological Survey Techniques and Methods 6-A16.
- Harding, C., 2007: *Upper South East Dryland Salinity and Flood Management Program Reflows Project Background Paper - Wetland Environmental Values*. Department of Water, Land and Biodiversity Conservation: Mt Gambier, South Australia.
- Harrington, G. A., P. G. Cook, and A. L. Herczeg, 2002: Spatial and temporal variability of ground water recharge in central Australia: A tracer approach. *Ground Water*, **40** (5), 518–527.
- Hatch, C. E., A. T. Fisher, J. Revenaugh, J. Constantz, and C. Ruehl, 2006: Quantifying surface water-groundwater interactions using time series analysis of streambed thermal records: Method development. *Water Resour. Res.*, **42** (10).
- Hatch, C. E., A. T. Fisher, C. R. Ruehl, and G. Stemler, 2010: Spatial and temporal variations in streambed hydraulic conductivity quantified with time-series thermal methods. *J. Hydrol.*, **389**, 276 – 288, doi:10.1016/j.jhydrol.2010.05.046.
- Hipólito, J. N. and J. M. Loureiro, 1988: Analysis of some velocity-area methods for calculating open channel flow. *Hydrol. Sci. J.*, **33** (3), 311 – 320, doi:10.1080/02626668809491250.
- Hoeksema, R. J. and P. K. Kitanidis, 1985: Analysis of the Spatial Structure of Properties of Selected Aquifers. *Water Resour. Res.*, **21** (8), 4W1532, doi:10.1029/WR021i004p00563.
- Hsu, M. H., J. C. Fu, and W. C. Liu, 2006: Dynamic Routing Model with Real-Time Roughness Updating for Flood Forecasting. *J. Hydraul. Eng. -ASCE*, **132** (6), 605 – 619, doi:10.1061/(ASCE)0733-9429(2006)132:6(605).

- Hubbell, J. M., J. B. Sisson, N. M. J., and R. G. Taylor, 2004: Well design to reduce barometric pressure effects on water level data in unconfined aquifers. *Vadose Zone J.*, **3** (1), 183–189.
- Hughes, J. D., C. D. Langevin, K. L. Chartier, and J. T. White, 2012: Documentation of the Surface-Water Routing (SWR1) Process for modeling surface-water flow with the U.S. Geological Survey Modular Ground-Water Model (MODFLOW-2005). *U.S. Geological Survey Techniques and Methods, book 6, chap.A40*, U.S. Geological Survey, 113 p.
- Iman, R. and J. Helton, 1988: An Investigation of Uncertainty and Sensitivity Analysis Techniques for Computer Models. *Risk Analysis*, **8** (1), 71–90, doi:10.1111/j.1539-6924.1988.tb01155.x.
- Irvine, D. J., P. Brunner, H. J. H. Franssen, and C. T. Simmons, 2012: Heterogeneous or homogeneous? Implications of simplifying heterogeneous streambeds in models of losing streams. *J. Hydrol.*, **424-425**, 16–23, doi:10.1016/j.jhydrol.2011.11.051.
- Jarrett, R. D., 1985: *Determination of Roughness Coefficients for streams in Colorado*. U. S. Geological Survey, Lakewood, Colorado.
- Jobson, H. E. and A. W. Harbaugh, 1999: *Modifications to the Diffusion Analogy Surface-Water Flow Model (Daflow) for Coupling to the Modular Finite-Difference Ground-Water Model (Modflow)*. U.S. Geological Survey Open-File Report 99-217, 107 p pp.
- Jolly, I., K. McEwan, and K. Holland, 2008: A review of groundwater-surface water interactions in arid/semi-arid wetlands and the consequences of salinity for wetland ecology. *Ecohyd.*, **1** (1), 43 –58, doi:10.1002/eco.6.
- Kalbus, E., F. Reinstorf, and M. Schirmer, 2006: Measuring methods for groundwater - surface water interactions: a review. *Hydrol. Earth Sys. Sc.*, **10** (6), 873–887, doi: 10.1007/s00767-008-0066-9.
- Kalbus, E., C. Schmidt, J. Molson, F. Reinstorf, and M. Schirmer, 2009: Influence of aquifer and streambed heterogeneity on the distribution of groundwater discharge. *Hydr. Earth Sys. Sc.*, **13** (1), 69 – 77.

- Kalbus, E., C. Schmidt, F. Reinstorf, R. Krieg, and M. Schirmer, 2008: How streambed temperatures can contribute to the determination of aquifer heterogeneity. *Grundwasser*, **13**, 91–100, doi:10.1007/s00767-008-0066-9.
- Kennedy, C. D., D. P. Genereux, D. R. Corbett, and H. Mitasova, 2009: Relationship among groundwater age, denitrification, and the coupled groundwater and nitrogen fluxes through a streambed. *Water Resour. Res.*, **45** (9), W09402, doi:10.1029/2008wr007400.
- Kennedy, C. D., D. P. Genereux, H. Mitasova, D. R. Corbett, and S. Leahy, 2008: Effect of sampling density and design on estimation of streambed attributes. *J. Hydrol.*, **355**, 164–180, doi:10.1016/j.jhydrol.2008.03.018.
- Kennedy, C. D., L. C. Murdoch, D. P. Genereux, D. R. Corbett, K. Stone, P. Pham, and H. Mitasova, 2010: Comparison of darcian flux calculations and seepage meter measurements in a sandy streambed in north carolina, united states. *Water Resour. Res.*, **46**, W09501, doi:10.1029/2009wr008342.
- Keppel, R. V. and K. G. Renard, 1962: Transmission losses in ephemeral stream beds. *J. of Hydraul. Div. Proc. Am. Soc. Civ. Eng.*, **355**, 164–180, doi:10.1016/j.jhydrol.2008.03.018.
- Khatibi, R. H., J. J. R. Williams, and P. R. Wormleaton, 2006: Identification problem of open-channel friction parameters. *J. Hydraul. Eng.-ASCE*, **123**, 1078–1088, doi:10.1061/(asce)0733-9429(1997)123:12(1078).
- Kim, K. Y., T. Kim, Y. Kim, and N. C. Woo, 2007: A semi-analytical solution for groundwater responses to stream-stage variations and tidal fluctuations in a coastal aquifer. *Hydrol. Proc.*, **21** (5), 665–674, doi:10.1002/hyp.6255.
- Knighton, A. D. and G. C. Nanson, 1994: Flow transmission along an arid zone anastomosing river, cooper creek, australia. *Hydrol. Proc.*, **8**, 137–157, doi:10.1002/hyp.3360080205.
- Koussis, A. D., E. Akylas, and K. Mazi, 2007: Response of sloping unconfined aquifer

- to stage changes in adjacent stream: II. Applications. *J. Hydrol.*, **338**, 73–84, doi: 10.1016/j.jhydrol.2007.02.021.
- Landon, M., D. Rus, and F. Harvey, 2001: Comparison of Instream Methods for Measuring Hydraulic Conductivity in Sandy Streambeds. *Ground Water*, **39 (6)**, 870 – 885, doi:10.1111/j.1745-6584.2001.tb02475.x.
- Lee, S. Y., S. F. Calre, and G. E. Fogg, 2007: Geologic heterogeneity and a comparison of two geostatistical models: Sequential gaussian and transition probability-based geostatistical simulations. *Adv. Water Resour.*, **30**, 1914 – 1932, doi: 10.1016/j.advwatres.2007.03.005.
- Logani, K. L., 1985: Piezometer installation under artesian conditions - closure. *J. Geotech. Eng.-ASCE*, **111 (11)**, 1351–1352.
- Maidment, D. R., 1992: *Handbook of Hydrology*). McGraw-Hill, New York, 1424 p pp.
- Mariethoz, G. and B. F. J. Kelly, 2011: Modelling complex geological structures with elementary training images and transform-invariant distances. *Water Resour. Res.*, **47**, W07527, doi:10.1029/2011WR010412.
- Mariethoz, G., P. Renard, and J. Strabhaar, 2010: The Direct Sampling method to perform multiple-point geostatistical simulations. *Water Resour. Res.*, **46**, W11526, doi: 10.1029/2008WR007621.
- McCallum, J. L., P. G. Cook, D. Berhane, C. Rumpf, and G. A. McMahon, 2012: Quantifying groundwater flows to streams using differential flow gaugings and water chemistry. *J. Hydrol.*, (**416-418**), 118–132, doi:10.1016/j.jhydrol.2011.11.040.
- McCord, J., C. Gotway, and S. Conrad, 1997: Impact of geologic heterogeneity on recharge estimation using environmental tracers: numerical modeling investigation. *Water Resour. Res.*, **33 (6)**, 1229 –1240, doi:10.1029/96wr03755.
- Millham, N. P. and B. L. Howes, 1995: A Comparison of methods to determine K in shallow coastal aquifer. *Ground Water*, **33 (1)**, 49–57, doi:10.1111/j.1745-6584.1995.tb00262.x.

- Moench, A. F. and P. M. Barlow, 2000: Aquifer response to stream-stage and recharge variations. I. Analytical step-response functions. *J. Hydrol.*, **230** (3), 192 – 210.
- Morin, E., et al., 2009: Flood routing and alluvial aquifer recharge along the ephemeral arid Kuiseb River, Namibia. *J. Hydrol.*, **368** (1), 262–275, doi: 10.1016/j.jhydrol.2009.02.015.
- Morvan, H., D. Knight, N. Wright, X. Tang, and A. Crossley, 2008: The concept of roughness in fluvial hydraulics and its formulation in 1D, 2D, and 3D numerical simulation models. *J. Hydraul. Res.*, **46** (2), 191–208.
- Moussa, R. and C. Bocquillon, 1996: Criteria for the choice of flood-routing methods in natural channels. *J. Hydrol.*, **186** (1-4), 1–30, doi:10.1016/s0022-1694(96)03045-4.
- Mudd, S. M., 2006: Investigation of the hydrodynamics of flash floods in ephemeral channels: Scaling analysis and simulation using a shock-capturing flow model incorporating the effects of transmission losses. *J. Hydrol.*, **324** (1-4), 65–79, doi: 10.1016/j.jhydrol.2005.09.012.
- Niswonger, R. G., S. Panday, and M. Ibaraki, 2011: *MODFLOW-NWT, A Newton formulation for MODFLOW-2005*. U.S. Geological Survey Techniques and Methods 6-A37.
- Niswonger, R. G. and D. E. Prudic, 2004: Modeling variably saturated flow using kinematic waves in MODFLOW. *Groundwater Recharge in a Desert Environment: The Southwestern United States*, J. Hogan, F. Phillips, and B. Scanlon, Eds., American Geophysical Union, 379–396.
- Niswonger, R. G. and D. E. Prudic, 2005: *Documentation of the Streamflow-Routing (SFR2) Package to include unsaturated flow beneath streams- A modification to SFR1*. U.S. Geological Survey Techniques and Methods 6-A13.
- Niswonger, R. G., D. E. Prudic, G. E. Fogg, D. A. Stonestrom, and E. M. Buckland, 2008: Method for estimating spatially variable seepage loss and hydraulic conductivity in intermittent and ephemeral streams. *Water Resour. Res.*, **44** (5), W05418, doi: 10.1029/2007wr006626.

- Niswonger, R. G., D. E. Prudic, G. Pohll, and J. Constantz, 2005: Incorporating seepage losses into the unsteady streamflow equations for simulating intermittent flow along mountain front streams. *Water Resour. Res.*, **41** (6), W06006, doi:10.1029/2004wr003677.
- Panday, S. and P. S. Huyakorn, 2004: A fully coupled physically-based spatially-distributed model for evaluating surface/subsurface flow. *Adv. Water Resour.*, **27** (4), 361–382, doi:10.1016/j.advwatres.2004.02.016.
- Parsons, S., R. Evans, and M. Hoban, 2008: Surface-groundwater connectivity assessment . *A report to the Australian Government from the CSIRO Murray-Darling Basin Sustainable Yields Project*, 35.
- Passalacqua, P., P. Belmont, and E. Foufoulla-Georgiou, 2012: Automatic geomorphic feature extraction from lidar in flat and engineered landscapes. *Water Resour. Res.*, **48** (3), doi:10.1029/2011WR010958.
- Philip, J. R., 1957: The theory of infiltration, 1. the infiltration equation and its solution. *Soil Sc.*, **53**, 333–337.
- Philip, J. R., 1958: The theory of infiltration, 7. the infiltration equation and its solutionn. *Soil Sc.*, **85**, 345–357.
- Pilgrim, D., T. Chapman, and D. Doran, 1988: Problems of rainfall-runoff modeling in arid and semi-arid regions. *Hydrol. Sc. J.*, **33** (4), 379 – 400, doi:10.1080/02626668809491261.
- Pool, D. R. and J. H. Eychaner, 1995: Measurements of aquifer-storage change and specific yield using gravity surveys. *Groundwater*, **33**, 425–432, doi:10.1111/j.1745-6584.1995.tb00299.x.
- Post, V. and J. Von Asmuth, 2013: Review: Hydraulic head measurements-new technologies, classic pitfalls. *Hydrogeol. J.*, **21** (4), 737–750.
- Price, M., 2009: Barometric water-level fluctuations and their measurement using vented

- and non-vented pressure transducers. *Quat. J. Eng. Geol. Hydrogeol.*, **42**, 245–250, doi:10.1144/1470-9236/08-084.
- Ragab, R. and C. Prudhomme, 2002: Climate change and water resources management in arid and semi-arid regions: prospective and challenges for the 21st century. *Biosys. Eng.*, **81 (1)**, 3–34, doi:10.1006/bioe.2001.0013.
- Rasmussen, T. C. and L. A. Crawford, 1997: Identifying and removing barometric pressure effects in confined and unconfined aquifers. *Ground Water*, **35 (3)**, 502–511, doi:10.1111/j.1745-6584.1997.tb00111.x.
- Rogers, G. D. and D. R. Moore, 1997: Drilling, sampling, and construction of monitoring wells under flowing artesian conditions. *Env. Eng. Geosc.*, **3 (3)**, 369–373.
- Rorabaugh, M. I., 1964: Estimating changes in bank storage and ground-water contribution to streamflow. *IAHS publication*, **63**, 432 – 441.
- Rosenberry, D. and J. LaBaugh, 2008: *Field techniques for estimating water fluxes between surface water and groundwater*. U.S. Geological Survey Techniques and Methods 4-D2.
- Rötting, T. S., J. Carrera, J. Bolzicco, and J. M. Salvany, 2006: Stream-Stage Response Tests and Their Joint Interpretation with Pumping Tests. *Ground Water*, **44 (3)**, 371–385, doi:10.1111/j.1745-6584.2005.00138.x.
- Ruehl, C., A. T. Fischer, C. Hatch, M. L. Huertos, G. Stemler, and C. Shennan, 2006: Differential gauging and tracer tests resolve seepage fluxes in a strongly-losing stream. *J. Hydrol.*, **330 (1-2)**, 235–248, doi:10.1016/j.jhydrol.2006.03.025.
- Saltelli, A., M. Ratto, T. Andres, F. Campolongo, J. Cariboni, D. Gatelli, M. Saisana, and S. Tarantola, 2008: *Global Sensitivity Analysis. The Primer*. John Wiley and Sons, Ltd.
- Sanchez-Vila, X., A. Guadagnini, and J. Carrera, 2006: Representative hydraulic conductivities in saturated groundwater flow. *Rev. Geophys.*, **44 (3)**, RG3002, doi:10.1029/2005RG000169.

- Scaloppi, E. J., G. P. Merkley, and L. S. Willardson, 1995: Intake parameters from advance and wetting phases of surface irrigation. *J. Irr. Drain. Eng.-ASCE*, **121**, 57–70, doi:10.1061/(asce)0733-9437(1995)121:1(57).
- Scanlon, B., R. Healy, and P. Cook, 2002: Choosing appropriate techniques for quantifying groundwater recharge. *Hydrogeol. J.*, **10 (1)**, 18 –39, doi:10.1007/s10040-001-0176-2.
- Scanlon, K., B. Keese, A. Flint, L. Flint, C. Gaye, W. Edmunds, and I. Simmers, 2006: Global synthesis of groundwater recharge in semiarid and arid regions. *Hydrol. Proc.*, **20 (15)**, 3335 –3370, doi:10.1002/hyp.3665.
- Schmidt, C., A. Musolff, N. Trauth, M. Vieweg, and J. H. Fleckenstein, 2012: Transient analysis of fluctuations of electrical conductivity as tracer in the stream bed. *HESS*, **16**, 3689 – 3697.
- Serrano, S. E., S. R. Workman, K. Srivastava, and B. M. V. Cleave, 2007: Models of nonlinear stream aquifer transients. *J. Hydrol.*, **336**, 199 – 205, doi:10.1016/j.jhydrol.2007.01.016.
- Shanfield, M. and P. Cook, in press: Transmission losses, infiltration and groundwater recharge through ephemeral and intermittent streambeds: a review of applied methods. *J. Hydrol.*
- Shanfield, M., R. G. Niswonger, D. E. Prudic, G. Pohll, R. Susfalk, and S. M. Panday, 2012: A method for estimating spatially-variable seepage and hydraulic conductivity in channels with very mild slope. *Hydrol. Proc.*, doi:10.1002/hyp.9545.
- Shanfield, M., G. Pohll, and R. Susfalk, 2010: Use of heat-based vertical fluxes to approximate total flux in simple channels. *Water Resour. Res.*, **46**, doi:10.1080/07438141.2010.504064.
- Sophocleous, M. A., 2002: Interactions between groundwater and surface water: The state of the science. *Hydrogeol. J.*, **10**, 52–67.

- Sophocleous, M. A., A. Koussis, J. Martin, and S. Perkins, 1991: Evaluation of simplified stream-aquifer depletion models for water rights administration. *J. Hydrol.*, **124**, 207 – 228, doi:10.1016/0022-1694(91)90015-a.
- Spane, F. A., 2002: Considering barometric pressure in groundwater flow investigations. *Water Resour. Res.*, **38**, 6, doi:10.1029/2001wr000701.
- Spanoudaki, K., A. Nanou-Giannarou, Y. Paschalinos, C. D. Memos, and A. I. Stamou, 2010: Analytical solutions to the stream-aquifer interaction problem: a critical review. *Glob. Nest. J.*, **12** (2), 126 – 139.
- Sprecher, S. W., 2008: Installing monitoring wells in soils (version 1.0). *Natural Resources Conservation Service*, U. S. D. A., Lincoln, NE.
- Stonedahl, S. G., J. W. Harvey, A. Wörman, M. Salehin, and P. A. I., 2010: A multiscale model for integrating hyporheic exchange from ripples to meanders. *Water Resour. Res.*, **46**, W12539, doi:10.1029/2009WR008865.
- Su, G. W., J. Jasperse, D. Seymour, and J. Constantz, 2004: Estimation of hydraulic conductivity in an alluvial system using temperatures. *Ground Water*, **42** (6), 890–901.
- Toth, J., 1970: A conceptual model of the groundwater regime and the hydrogeologic environment. *J. Hydrol.*, (10), 164 – 176.
- USACE, 1991: Hydrographic surveying. *Engineer Manual EM 1110-1003*, Washinton, DC.
- USACE, 2005: Technical standard for water-table monitoring of potential wetland sites. *ERDC TN-WRAP-05-2*, US Army Engineer Research and Development Center.
- Vanderzalm, J. L., B. M. Jeuken, J. D. H. Wischusen, P. Pavelic, C. L. La Salle, A. Knapton, and P. J. Dillon, 2011: Recharge sources and hydrogeochemical evolution of groundwater in alluvial basins in arid central Australia. *J. Hydrol.*, **397**, 71–82, doi:10.1016/j.jhydrol.2010.11.035.

- Vieira, J. H. D., 1983: Conditions governing the use of approximations for the Saint-Venant equations for shallow surface water flow. *J. Hydrol.*, **60**, 43–58, doi:10.1016/0022-1694(83)90013-6.
- Walters, M. O., 1990: Transmission losses in arid regions. *J. Hydraul. Eng.-ASCE*, **116** (1), 129–138, doi:10.1061/(asce)0733-9429(1990)116:1(129).
- Ward, K. L., 1974: *The underground water of the south-eastern part of South Australia*. Geological Survey of South Australia, Bulletin No. 19.
- Waterhouse, J. D., M. A. Cobb, , and G. S. of South Australia, 1977: *The geology and hydrogeology of the South-East province, South Australia: a bibliography*. Dept. of Mines, Geol. Survey of S. A., Adelaide.
- Weeks, E. P., 1979: Barometric fluctuations in wells tapping deep unconfined aquifers. *Water Resour. Res.*, **15**, 1167–1176, doi:10.1029/WR015i005p01167.
- Winter, T. C., J. W. Harvey, O. L. Franke, and W. M. Alley, 1998: *Ground Water and Surface Water: A Single Resource*. U.S. Geological Survey Circular 1139, Denver, Colorado.
- Wojnar, A., S. Mutiti, and J. Levy, 2013: Assessment of geophysical surveys as a tool to estimate riverbed hydraulic conductivity. *J. Hydrol.*, **482**, 40 – 56, doi:10.1016/j.jhydrol.2012.12.018.
- Wood, B. D., 2009: The role of scaling laws in upscaling. *Adv. Water Res.*, **32** (5), 723–736, doi:10.1016/j.advwatres.2008.08.015.
- Woolhiser, D. A., 1974: *Unsteady Flow in Open Channels: Proceedings of Institute on Unsteady Flow in Open channels*. Colorado State University, Water Resources Publications, Fort Collin, Colorado.
- Yeh, T. C. J., C. H. Lee, K. C. Hsu, and Y. C. Tan, 2007: Fusion of active and passive hydrologic and geophysical tomography surveys: The future of subsurface characterization. *Data Interogation in Subsurface Hydrology, Geophys. Monogr. Ser.*, D. Hyndman, F. day Lewis, and K. Singha, Eds., AGU, Washington, D. C., 109–120.

Yeh, T. C. J., J. Xiang, R. M. Suribhatla, C. H. Hsu, K. C. and Lee, and J. C. Wen, 2009: River stage tomography: A new approach for characterizing groundwater basins. *Water Resour. Res.*, **45**, W05409, doi:10.1029/2008wr007233.

Zinn, B. and C. F. Harvey, 2003: When good statistical models of aquifer heterogeneity go bad: A comparison of flow, dispersion, and mass transfer in connected and multivariate Gaussian hydraulic conductivity fields. *Water Resour. Res.*, **39** (3), 1051, doi:10.1029/2001WR001146.

Zlotnik, V. A. and H. Huang, 1999: Effects of shallow penetration and streambed sediments on aquifer response to stream stage fluctuations (analytical model). *Ground Water*, **37** (4), 599–605.

# Appendices



# Chapter A

## Analytical model validation

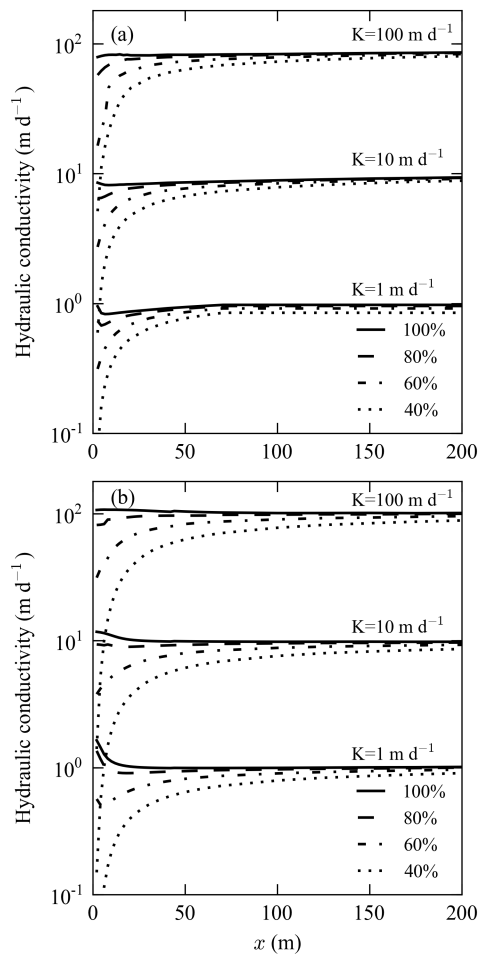


Figure A.1: Influence of aquifer thickness ((a) 10 m and (b) 100 m) and stream penetration (40-100%) on determining hydraulic conductivities using the Hall and Moench (1972) analytical solution. Input data was derived from homogenous 2-dimensional (cross sectional) aquifers simulated in MODFLOW, distance between stream and observation well was identical to the heterogeneous model.

The effect of violating the constant transmissivity assumption in the Hall and Moench (1972) analytical model are shown in Figure A.1. If the stream is assumed to fully penetrate the aquifer, the error in the estimation of  $K_{eff}$  is equal to the change in transmissivity relative to the aquifer depth i.e., the error for a fully penetrating stream in a 10 m aquifer

where the change in stream level and observation well response are 1.5 m will be 15%. The degree of stream penetration is only important when the well is less than 50 m from the channel. Therefore in such a situation, the error in the Hall and Moench (1972) analytical model is contingent upon the conceptualization of the depth of stream penetration. The error in  $K_{eff}$  is greatest when the well is less than 20 m from the stream, at these distances hydraulic conductivity can be underestimated by an order of magnitude. Under these conditions, the use of alternative analytical models (Zlotnik and Huang, 1999; Barlow et al., 2000; Kim et al., 2007) or a numerical model may therefore provide a better estimate of hydraulic conductivity. These findings are in agreement with those of Birkhead and James (2002).

# Chapter B

## Further Discussion of Sensitivity Analysis

### B.1 Distribution of sensitivity analysis results in Figure 3.8

The results in Figure 3.8 appear to have an upper and lower bound, the upper bound being more apparent in the results of the *ff* flow and *sws*  $\phi$  values. The upper bound in the  $\phi$  values are a result of successful runs (i.e., within the convergence criteria) where the flood front was unable to reach the segment boundaries (flow was less than  $0.05 \text{ m}^3\text{s}^{-1}$ ) within the time steps. For example, where the flood front progressed down the channel at a slower rate, the *ff* flow at each of the boundaries would be on the order of  $0.002 \text{ m}^3\text{s}^{-1}$ , substantially lower than  $0.05 \text{ m}^3\text{s}^{-1}$ . Therefore the difference between the observed and modelled flow would be consistently large resulting in a consistent  $\phi$  value for *ff* flow. Similarly, the groundwater response and surface water stage response would be delayed or not present, also resulting in a large difference between the observed and modelled data.

### B.2 Assymetry in $\phi$ values for $S_y$

The asymmetry in the  $S_y$  parameter range in Figure 3.8 and 3.10 is a result of elimination of non-convergent model runs. The parameter values for  $S_y$  were therefore have been increased by upto approx. +75% of the  $S_y$  value (approx. 3 standard deviations). Table 3.2 shows the range of  $S_y$  values used for the site to be small (varying from 0.02-0.18), an increase in these values causes an increase in the  $\phi$  values particularly for *sws*. High  $S_y$  fits *gwh* but does affect *sws*. The results appear to suggest that the fit to *gwh*  $\phi$

would deteriorate with a decrease in  $S_y$  values. Although, this is limited by the number of convergent model runs were the  $S_y$  value has been reduced.

The influence of the  $S_y$  value range on the phi values appear to be limited. Only the response in the  $h_g^i$  for  $gwh \phi$  appears to be slightly different from that of the other parameters, this maybe a result of the asymmetry in the  $S_y$  values. However due to the antecedent moisture conditions within the channel (high moisture content) the influence of the  $S_y$  asymmetry may have had limited impact on the results. If the channel were very dry prior to the flow event, asymmetry in the  $S_y$  would likely have a more significant impact.

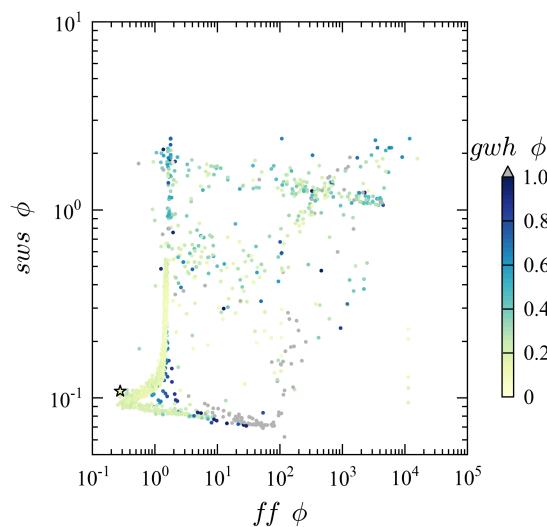


Figure B.1: The relation between flood front flow  $\phi$ , surface water stage  $\phi$ , and ground-water head  $\phi$  (colour bar for reference). Star represents the calibrated model  $\phi$ .

### B.3 Calibrated model $\phi$ values compared to the sensitivity analysis $\phi$ results

The location of the calibrated models  $\phi$  values compared to those obtained from the LHS analysis may be due to none of the successful runs recreate similar conditions to the calibrated model, had there been more model runs, (e.g.  $10^{27}$  as would be recommended given the 27 parameters included in the analysis) the cloud of runs may extend to the calibrated run (star Figure 3.9) . Figure B.1 shows how the calibrated model  $\phi$  values compare for the  $ff$  flow and  $sws$ . The star falls just on top of the cloud, possibly indicating

that there was greater similarity (in terms of low  $\phi$  values) between models runs for the *ff* flow and *sws*, than for the *gwh*  $\phi$  values.

## B.4 Discussion on the impact of Manning's $n$

Reference to the importance of Manning's  $n$  in the Chapter 5 arises from 2 points. The precursor to this model (Niswonger et al., 2008) using the kinematic wave approach) identified that Manning's  $n$  was an importance parameter when they conducted a sensitivity analysis of their model. We conducted a similar one-at-a-time sensitivity analysis on the Western Reflows Floodway model which also identified that Manning's  $n$  was important. During the review process of this manuscript, it was suggested that a more robust (and demonstrative) sensitivity analysis be undertaken, hence the use of the Latin Hypercube sensitivity (LHS) Monte Carlo approach. The results of which showed the importance of Manning's  $n$  to be low, this may be a result of the conditions within the channel prior to the flow event (high moisture content within the streambed sediments). We have also used relatively small Manning's  $n$  values relative to those found in the natural environment, this may account of the minimal impact for this model. In natural channels, where there are higher hydraulic conductivities of the streambed sediments and drier antecedent conditions, the need to accurately capture Manning's  $n$  may prove highly important.

Further improvement to the LHS analysis would involve investigating the correlation between the parameters included in the analysis. For the Western Reflows Floodway model, this would reveal which parameters result in the minimal sensitivity of the model to changes in the Manning's  $n$  value.



# **Chapter C**

## **Field data**

A CD of the field data used in Chapters 2, 3, and 4 is provided.